Frontiers in Bioscience Landmark

Front. Biosci. (Landmark Ed) **2026**; 31(7): 49673
https://doi.org/10.31083/FBL49673

Original Research

Integrative Bioinformatics and Experimental Validation Reveal that METTL9 Drives Lung Adenocarcinoma Progression via TGF-β/Smad-Mediated EMT Activation

Chen Gong[1,2,†], Yuyan Chen[2,†], Yuchen Xie[3], Yuling Liu[2], La Jiang[1], Haoyuan Jiang[3], Zhijun Chen[4], Bin Yuan[1,*], Xueqin Zhang[3,4,*]

[1]Department of Pharmacology, School of Pharmaceutical Sciences, Anhui Medical University, 230032 Hefei, Anhui, China
[2]Clinical Research Center, Suzhou Hospital of Anhui Medical University, 234000 Suzhou, Anhui, China
[3]Department of Thoracic and Cardiac Surgery, Suzhou Hospital of Anhui Medical University, 234000 Suzhou, Anhui, China
[4]Department of Thoracic and Cardiac Surgery, Zhoushan Hospital of Wenzhou Medical University, 316000 Zhoushan, Zhejiang, China
*Correspondence: yuanbin@ahmu.edu.cn (Bin Yuan); zxqdreambj@163.com (Xueqin Zhang)
[†]These authors contributed equally.
*Corresponding authors: Xueqin Zhang is the primary corresponding author, Bin Yuan is the co-corresponding author.
Academic Editor: Esteban C. Gabazza
Submitted: 3 January 2026 Revised: 8 May 2026 Accepted: 27 May 2026 Published: 27 July 2026

Abstract

Background: Methyltransferase-like 9 (METTL9) has been implicated in tumor progression, yet its clinical significance, functional roles, and immunoregulatory functions in lung adenocarcinoma (LUAD) remain unclear. This study aimed to integrate multi-omics datasets and experimental evidence to systematically evaluate the expression profile, prognostic value, molecular mechanisms, and tumor microenvironment (TME)-related functions of METTL9 in LUAD. **Methods:** Transcriptome and clinical data for LUAD and METTL9 protein expression were obtained from public databases. Survival analysis was performed using Kaplan–Meier analysis and Cox proportional hazards models. METTL9-related differentially expressed genes (DEGs) were screened, followed by functional annotation and pathway enrichment analysis. A protein-protein interaction (PPI) network associated with METTL9 was constructed using STRING. METTL9 gene mutations and promoter methylation levels were analyzed via cBioPortal and UALCAN. Immune infiltration was evaluated through gene set variation analysis (GSVA) and the TIMER platform. The role of METTL9 depletion in regulating transforming growth factor-β (TGF-β)/Smad signaling, epithelial-mesenchymal transition (EMT), as well as the behavior of A549 and H1975 cells was investigated. **Results:** METTL9 was markedly elevated in LUAD, which was confirmed in external datasets and immunohistochemistry. Increased METTL9 expression showed a strong association with advanced TNM stage, unfavorable clinicopathological parameters, and poor survival outcomes in univariate analysis. Receiver operating characteristic (ROC) analysis indicated that METTL9 showed moderate diagnostic utility for LUAD, with an Area Under the Curve (AUC) of 0.704 (95% Confidence Interval [CI]: 0.650–0.758) in the The Cancer Genome Atlas (TCGA) dataset and 0.815 (95% CI: 0.758–0.872) in the GSE31210 dataset. Moreover, high METTL9 expression was significantly correlated with poor survival outcomes (Hazard Ratio [HR] = 1.349, 95% CI: 1.010–1.802, $p = 0.043$). METTL9 interacted with multiple oncogenic proteins in the PPI network and showed significant correlations with cuproptosis-related genes. Immune infiltration analysis further demonstrated that METTL9 expression showed significantly associated with immune cell infiltration and the tumor immune microenvironment in LUAD. METTL9 knockdown suppressed LUAD cell proliferation, migration, invasion, and EMT, while promoting apoptosis and reducing the expression of B-cell lymphoma 2 (Bcl-2), phosphorylated Smad2 (p-smad2), and phosphorylated Smad3 (p-smad3). **Conclusion:** METTL9 is upregulated in LUAD and correlates with an unfavorable prognosis. Our results indicate that METTL9 may contribute to LUAD progression and EMT, potentially in relation to the TGF-β/Smad signaling pathway.

Keywords: METTL9; epithelial-mesenchymal transition; transforming growth factor beta; Smad proteins; tumor biomarkers; cuproptosis; tumor microenvironment; immune infiltration; lung adenocarcinoma; genetics

1. Introduction

Lung adenocarcinoma (LUAD), the most common histological subtype of non-small cell lung cancer (NSCLC), remains one of the major causes of cancer-related mortality globally [1]. Notwithstanding significant progress in targeted and immunotherapeutic strategies, overall survival (OS) among LUAD patients is still unsatisfactory. This can be primarily ascribed to diagnosis at advanced stages, strong metastatic potential, and the development of resistance to therapy [2,3]. Therefore, identifying novel molecular regulators that contribute to LUAD progression is of great importance, as they could act as predictive biomarkers or targets for therapeutic intervention.

Accumulating evidence suggests that epigenetic and posttranscriptional modifications are essential for cancer progression [4]. Proteins belonging to the methyltransferase-like (METTL) family are increasingly acknowledged as important mediators of gene expression

through RNA and protein methylation pathways, especially N6-methyladenosine (m6A) modification [5,6]. Several METTL family members have been extensively studied with regard to cancer. For example, METTL3 promotes chemoresistance in lung cancer by enhancing mitochondrial uptake [7] and accelerates colorectal cancer progression through activation of the Janus Kinase 1/Signal Transducer and Activator of Transcription 3 (JAK1/STAT3) signaling pathway [8]. In addition, METTL3 regulates thyroid cancer differentiation and chemosensitivity via Paired box 8 (PAX8) modulation [9]. Similarly, METTL14 has been reported to suppress cancer stemness in gastric cancer by inhibiting the activity of the Activating Transcription Factor 5/WD Repeat Domain 74 (ATF5/WDR74/β-catenin axis) [10] and to regulate glycolytic metabolism in colorectal cancer [11]. These findings highlight the diverse roles of METTL family members in tumor initiation, metastasis, and therapeutic response.

In contrast to the well-characterized roles of METTL3 and METTL14, the biological functions of methyltransferase-like 9 (METTL9) in cancer remain relatively poorly understood. METTL9 has recently been identified as a histidine methyltransferase that catalyzes 1-methylhistidine modification on specific protein substrates, potentially regulating protein stability and signaling pathways [12]. Recent studies have started to elucidate the potential involvement of METTL9 in tumor biology [13]. For instance, a circular RNA derived from METTL9 has been shown to facilitate colorectal cancer progression through sequestration of miR-551b-5p and subsequent upregulation of Cyclin-Dependent Kinase 6 (CDK6) expression [14]. Additionally, the Solute Carrier Family 7 Member 11 (METTL9–SLC7A11) axis has been reported to suppress ferroptosis and promote hepatocellular carcinoma progression [15]. However, whether METTL9 participates in lung cancer development, particularly in LUAD, has not yet been systematically investigated.

Epithelial–mesenchymal transition (EMT) is a critical biological process that drives epithelial tumor cells toward a mesenchymal phenotype, resulting in increased migration, invasion, and metastatic potential [4]. Among the signaling pathways that regulate EMT, the transforming growth factor-β (TGF-β) pathway is considered a key driver of EMT during cancer progression. Activation of TGF-β receptors induces phosphorylation of phosphorylated Smad2 (p-Smad2)and phosphorylated Smad3 (p-Smad3), which then associate with phosphorylated Smad4 (p-Smad4) and translocate into the nucleus to regulate the expression of EMT-related genes [16]. This signaling cascade is critically involved in tumor invasion, metastasis, and therapeutic resistance in multiple cancers, including LUAD [17].

On the basis of these observations, we hypothesized that METTL9 may be associated with LUAD progression and EMT-related signaling pathways, potentially involving the TGF-β/Smad pathway. Although the precise substrates of METTL9 in this pathway remain unknown, its activity as a histidine methyltransferase suggests that it may influence key signaling components or downstream regulatory proteins involved in EMT. In this study, a comprehensive integrative approach incorporating multiomics datasets, clinical data, as well as experimental validation results was applied to systematically explore the expression patterns, prognostic significance, molecular mechanisms, and tumor microenvironment (TME)-related roles of METTL9 in LUAD. Furthermore, functional experiments were conducted to determine whether METTL9 regulates EMT and the TGF-β/Smad signaling pathway in LUAD cells. Our results seek to define the biological role of METTL9 in LUAD and provide further insights into its utility as a prognostic marker and candidate therapeutic target.

2. Materials and Methods

2.1 Data Sources and Preprocessing

Transcriptomic and clinical data of LUAD were retrieved from The Cancer Genome Atlas (TCGA) via UCSC Xena. Normal lung RNA-seq data were obtained from the Genotype-Tissue Expression (GTEx) database, and proteomic profiles were obtained from the Clinical Proteomic Tumor Analysis Consortium (CPTAC) database. The external validation cohort (GSE31210) was downloaded from Gene Expression Omnibus (GEO). To improve cross-platform comparability, TCGA and GTEx expression data were normalized to Transcripts Per Million (TPM) values and subsequently log2-transformed. Batch effects associated with sequencing platforms and processing pipelines were adjusted using the ComBat algorithm in the *sva* package (v3.54.0, Baltimore, MD, USA). For TCGA-LUAD, only primary tumor samples with available RNA-seq data and complete survival information were retained; cases with missing OS data or duplicates were removed. CPTAC samples were filtered to include those with both proteomic profiles and corresponding clinical annotations. For GSE31210, only primary LUAD samples with expression and survival data were included, while incomplete records were excluded.

2.2 Survival Analysis

Kaplan–Meier survival analysis was used to assess the association between METTL9 expression and OS in LUAD patients. The optimal cutoff for stratifying METTL9 expression into high- and low-expression groups was identified using the *surv_cutpoint* function from the R package (v0.4.9, https://rpkgs.datanovia.com/survminer/index.html) *survminer*, based on maximally selected rank statistics. A 10-fold cross-validation approach was applied to minimize overfitting during cutoff determination. Independent prognostic factors were identified using univariate and multivariate Cox proportional hazards models. The propor-

tional hazards assumption was evaluated using Schoenfeld residuals via the *cox.zph* function in the R package *survival*.

2.3 Nomogram Construction and Validation

A prognostic nomogram was constructed using the R package *rms* by integrating independent prognostic variables identified through multivariate Cox regression analysis. Model performance in prediction was measured using the concordance index (C-index). A bootstrap resampling approach with 1000 repetitions was used for internal model validation to limit overfitting. Calibration curves were employed to evaluate the consistency between predicted and observed survival probabilities at 1, 3, and 5 years.

2.4 Differential Gene Expression Analysis

Gene expression differences between LUAD tumors and normal lung tissues were analyzed using the R package *DESeq2*. Raw count RNA sequencing data retrieved from the TCGA database were processed with *DESeq2* to ensure statistical validity of the negative binomial distribution model. Genes were defined as differentially expressed (DEGs) when adjusted p values were <0.05 and |log2 fold change| exceeded 1. TPM-normalized data were used for downstream visualization and comparative analyses of transcript abundance.

2.5 Functional Enrichment Analysis

Using the R package *clusterProfiler*, gene set enrichment analysis (GSEA) was performed to detect biological pathways potentially associated with METTL9 expression. Genes were sorted by log2 fold change comparing high and low METTL9 expression groups. The number of permutations was set to 1000, and the enrichment significance was evaluated using the normalized enrichment score (NES). The Benjamini–Hochberg (BH) procedure was employed to account for multiple testing and to control the false discovery rate (FDR). Pathways satisfying FDR <0.25 and adjusted $p < 0.05$ were considered significantly enriched.

2.6 Protein–Protein Interaction (PPI) Network Analysis

A protein–protein interaction (PPI) network was constructed using the STRING database (version 11.5, https://string-db.org/) to explore potential interactions among METTL9-related proteins. Only interactions with a confidence score ≥0.4 (medium confidence) were included to improve reliability. Visualization and analysis of the interaction network were performed using Cytoscape (v3.10.2, https://cytoscape.org/), excluding nodes with no interactions from the final network.

2.7 Gene Mutation and DNA Methylation Analysis

METTL9 mutations and copy number variations (CNVs) in LUAD were analyzed using the cBioPortal database. Based on METTL9 mutation status, patients were classified into mutation and wild-type groups. Kaplan–Meier survival analysis and the log-rank test were used to assess differences in survival between the two groups. METTL9 promoter methylation levels in LUAD were additionally evaluated based on data from the UALCAN database (http://ualcan.path.uab.edu).

2.8 Immune Infiltration Analysis

Enrichment scores for 24 immune cell types were derived using the gene set variation analysis (GSVA) method. Associations between METTL9 expression and immune cell infiltration, as well as KRAS and Programmed Cell Death Protein 1 (PDCD1) expression, were assessed using Spearman correlation analysis. The Wilcoxon rank-sum test was performed to assess differences in immune infiltration levels between high- and low-METTL9 expression groups. Multiple testing across the 24 immune cell subsets was corrected using the BH procedure, and results with FDR <0.05 were regarded as statistically significant. In addition, Tumor Immune Estimation Resource (TIMER) database (http://cistrome.org/TIMER/) analysis was used to further validate the association between METTL9 expression and immune infiltration in LUAD. TIMER provides partial Spearman correlation analysis adjusted for tumor purity, which was employed in this study to reduce potential bias caused by tumor purity in immune infiltration estimates.

2.9 Immunohistochemistry (IHC)

The LUAD samples, together with matched non-tumorous tissues were collected from 10 LUAD patients in the Suzhou Hospital of Anhui Medical University. All the specimens were histopathologically confirmed as LUAD by two independent pathologists. The study was approved by the Ethics Committee of the Suzhou Hospital of Anhui Medical University (Approval No. KY-YJ-2025-014), and written informed consent was secured from all patients following the Declaration of Helsinki. LUAD samples and corresponding normal tissues were fixed in paraffin (8002-74-2; Nanjing Reagent, Nanjing, China) and then sectioned at a thickness of 5 μm. Antigen retrieval was carried out using citrate buffer (C2488; Sigma-Aldrich, MO, USA), followed by incubation of the sections with 5% bovine serum albumin for 1 hour (ST025; Beyotime, Shanghai, China). METTL9 primary antibody (83531-5-RR; 1:500 - 1:2000, Proteintech, Wuhan, China) was added overnight. Following this, the sections were incubated with the secondary antibody (ab6721; Abcam, Cambridge, UK) for 1 hour. After 3,3′-diaminobenzidine (DAB) staining (ab64238; Abcam, UK), hematoxylin counterstaining (H9627; Sigma–Aldrich, USA) was performed. The stained tissue sections were examined under an optical microscope (Nikon Eclipse 80i, Tokyo, Japan). The IHC staining was scored independently by two experienced pathologists without knowledge of the patients' clinical information. METTL9 expression levels were quantified using the H-score method, which in-

tegrates staining intensity (0–3) and the percentage of positively stained cells. The final H score was calculated as follows: H score = (percentage of cells with intensity 1 × 1) + (percentage of cells with intensity 2 × 2) + (percentage of cells with intensity 3 × 3), resulting in a score ranging from 0 to 300. ImageJ software (v1.54r, https://imagej.net) was used to quantify the staining intensity. On the basis of the median H score, the samples were classified into high- and low-METTL9 expression groups for subsequent analysis. Since the samples were paired, comparisons between tumor and corresponding normal tissues were performed using a paired *t* test. Values are reported as mean ± standard deviation (SD), and statistical significance was determined at $p < 0.05$ (two-sided).

2.10 Cell Lines and Transfection

BEAS-2B (SNL-203; Sunncell, Wuhan, China), IMR90 (STM-CL-5189; Stemcell, Shanghai, China), A549 (SNL-089; Sunncell, China), and H1975 (SNL-087; Sunncell, China) cells were grown in Dulbecco's modified Eagle's medium (DMEM; C0891; Beyotime, China) or RPMI-1640 medium (GNM31800; Genomcell, Hangzhou, China), both supplemented with 10% fetal bovine serum (FBS; 10100139; Thermo Fisher, Massachusetts, USA) and 1% penicillin–streptomycin (C0222; Beyotime, China). All cell lines were maintained at 37 °C in a humidified incubator with 5% CO_2 and routinely passaged every 2–3 days. Cells within 3–10 passages were used for all experiments to ensure experimental consistency. Lipo6000 (C0526; Beyotime, China) was used to transfect A549 and H1975 cells with small hairpin RNA (shRNA) targeting METTL9 (sh-METTL9#1, sh-METTL9#2, and sh-METTL9#3) or a negative control (sh-NC). Western blotting and Reverse Transcription-Quantitative Polymerase Chain Reaction (RT-qPCR) analyses were performed 48 hours after transfection to verify transfection efficiency. To further validate the specificity of the observed phenotypes and rule out potential off-target effects, all key experiments (cell viability, colony formation, migration, invasion, and apoptosis) were performed using at least two independent shRNA constructs (sh-METTL9#2 and sh-METTL9#3), and consistent results were obtained with both. Mycoplasma contamination testing was routinely performed on all cell lines prior to their use in experiments. All cell lines were validated by Short Tandem Repeat (STR) profiling and tested negative for mycoplasma.

2.11 Cell Viability

Cell viability was evaluated using a Cell Counting Kit-8 (CCK-8; 40203ES60; Yeasen, Shanghai, China). A549 and H1975 cells were plated in 96-well plates, followed by the addition of 10 µL CCK-8 reagent at 24, 48, and 72 h. The absorbance at 450 nm was determined using a microplate reader (Yomim, Hangzhou, China). All assays were conducted with at least three independent biological replicates, and each condition was tested in triplicate.

2.12 Colony Formation Assay

Transfected cells were plated in 6-well plates at a density of 800 cells per well and cultured for 2 weeks to allow colony formation, with medium replaced every 3 days. Colonies were fixed with 4% paraformaldehyde (E-IR-R114; Elabscience, Wuhan, China) for 10 min and stained with 0.5% crystal violet (MS4005; Maokangbio, Shanghai, China). Images were captured using a Nikon camera (Japan), and colony numbers were quantified using ImageJ software. A colony was defined as a cluster containing ≥50 cells, and only qualified colonies were included in the final analysis. All experiments were performed in triplicate with three independent biological replicates.

2.13 Transwell Migration and Invasion Assays

Migration ability of A549 and H1975 cells was evaluated using Transwell inserts (725121; Iallab, Shanghai, China), with 200 µL of cell suspension added to the upper chamber. The lower chamber was filled with culture medium supplemented with 10% FBS. Nonmigrating cells were extracted from the upper surface after 48 hours. Cells that reached the underside of the membrane were fixed with 4% paraformaldehyde and subsequently subjected to crystal violet staining. Prior to cell seeding, the upper chamber used for invasion assays was precoated with Matrigel (C0372; Beyotime, China) for 30 min at 37 °C. Matrigel-permeable cells were fixed and stained in a similar manner. Cells were examined using a microscope (Edmund Optics, Shenzhen, China), and five random fields per membrane were analyzed. Cell numbers were counted independently by two blinded investigators. Experiments were performed in triplicate.

2.14 Apoptosis Assay

Cell apoptosis was analyzed using an Annexin V-FITC/propidium iodide (PI) apoptosis detection kit (CX006; Epizyme, Shanghai, China). A549 and H1975 cells were collected, rinsed with ice-cold PBS, and resuspended in 195 µL of binding buffer. Annexin V-FITC and PI were then added and incubated for 15 min at room temperature in the dark. After incubation, 400 µL binding buffer was added, and apoptotic cells were detected using a flow cytometer (Agilent, CA, USA). Flow cytometry data were analyzed using standard gating strategy. Briefly, debris was excluded based on forward scatter (FSC) and side scatter (SSC) properties, and doublets were eliminated by FSC-A/FSC-H gating. Fluorescence compensation was applied according to single-stained controls, and quadrants for early and late apoptosis were defined based on unstained and single-stained controls. Data analysis was performed using FlowJo software (v10.0, BD Biosciences).

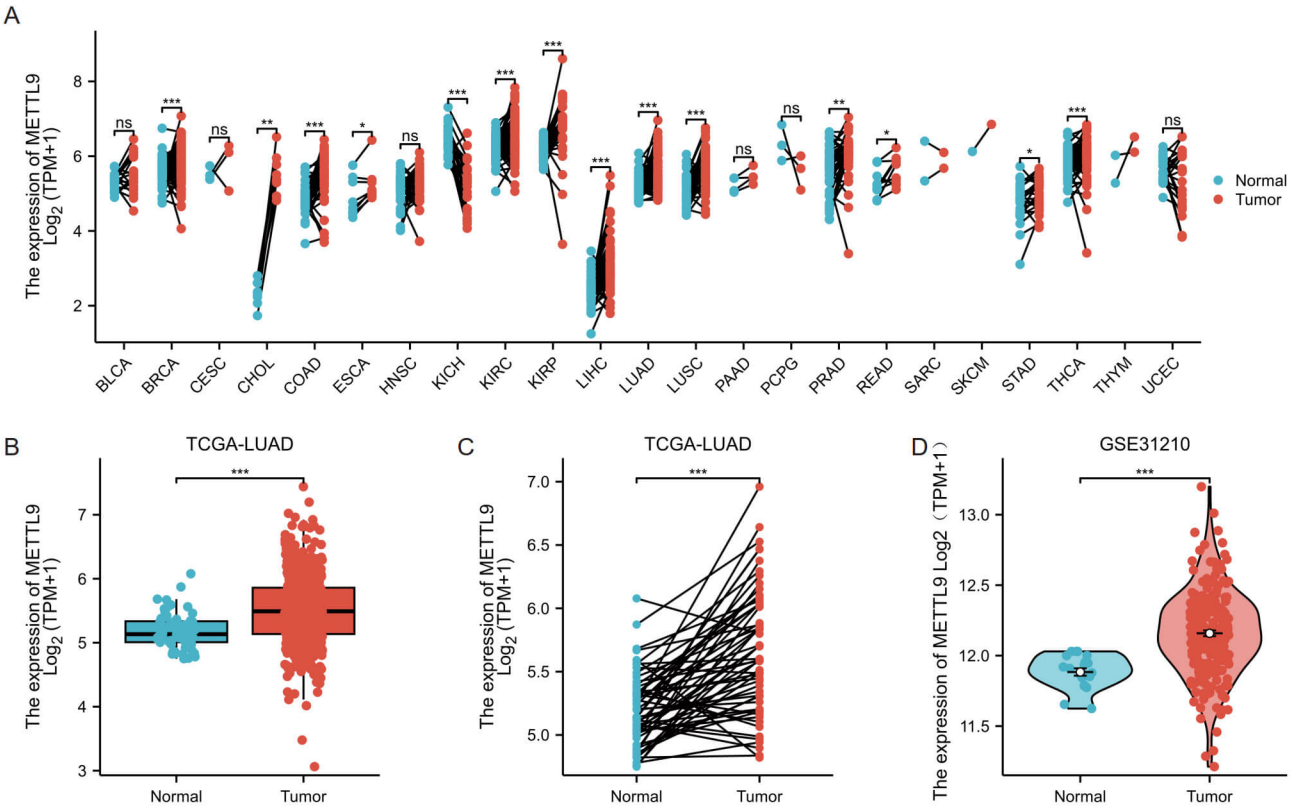

Fig. 1. Methyltransferase-like 9 (METTL9) expression across different cancers and in lung adenocarcinoma (LUAD). (A) Pan-cancer profiling of METTL9 using The Cancer Genome Atlas (TCGA) and Genotype-Tissue Expression (GTEx) databases. (B) TCGA-based analysis of METTL9 expression in LUAD versus normal lung tissues. (C) TCGA-based analysis of METTL9 expression in LUAD versus matched normal lung tissues. (D) Analysis of METTL9 expression in LUAD versus unpaired normal lung tissues using the GSE31210 dataset. ns: $p \geq 0.05$; *$p < 0.05$; **$p < 0.01$; ***$p < 0.001$.

2.15 Reverse Transcription-Quantitative Polymerase Chain Reaction (RT-qPCR)

Total RNA was obtained using TRIzol reagent (A33250; Thermo Fisher, USA). First-strand cDNA was prepared with a reverse transcription kit (04379012001; Roche, Basel-Stadt, Switzerland). RT-qPCR was conducted using an ABI PRISM 7300 system (Applied Biosystems, CA, USA) with SYBR Green PCR Master Mix (Thermo Fisher, USA), and the primer sequences are provided in **Supplementary Table 1**. β-actin was employed as the reference gene for normalization, and relative expression was quantified via the $2^{-\Delta\Delta Ct}$ method. All assays were carried out in three independent biological replicates.

2.16 Western Blotting

Cells were first lysed using Radio-Immunoprecipitation Assay (RIPA) buffer (P0013; Beyotime, China) and then sonicated. The supernatants were collected by centrifuging the lysates. To determine the protein concentration, a bicinchoninic acid (BCA, MA0082, Meilunbio, Dalian, China) test was performed. Proteins were fractionated on 10% SDS–PAGE gels (P0690; Beyotime, China) and then electrotransferred onto PVDF membranes (FFP24; Beyotime, China). Membranes were blocked in 5% nonfat milk for 1 hour, then incubated with primary antibodies (**Supplementary Table 2**) overnight, and further incubated with secondary antibodies for 1 hour. β-actin was employed as the loading control to assess protein loading consistency. Detection of protein bands was performed using an enhanced chemiluminescence (ECL) reagent (KGC4603; Keygene, Shanghai, China), with densitometric analysis carried out in ImageJ software. β-actin was used for normalization, and protein expression was quantified as fold changes relative to control samples. Each Western blot experiment was repeated independently at least three times.

2.17 Statistical Analysis

Data analyses were carried out using R software (version 4.2.1, https://www.r-project.org/), GraphPad Prism 9.0 (https://www.graphpad.com/), and IBM SPSS Statistics 26 (https://www.ibm.com/analytics/spss-statistics-software). Bioinformatics analyses were performed in R (version 4.2.1) using the *survival*, *survminer*, *ggplot2*, *clusterProfiler*, and *DESeq2* packages. The Wilcoxon rank-sum test and paired *t*-test were applied for unpaired and paired

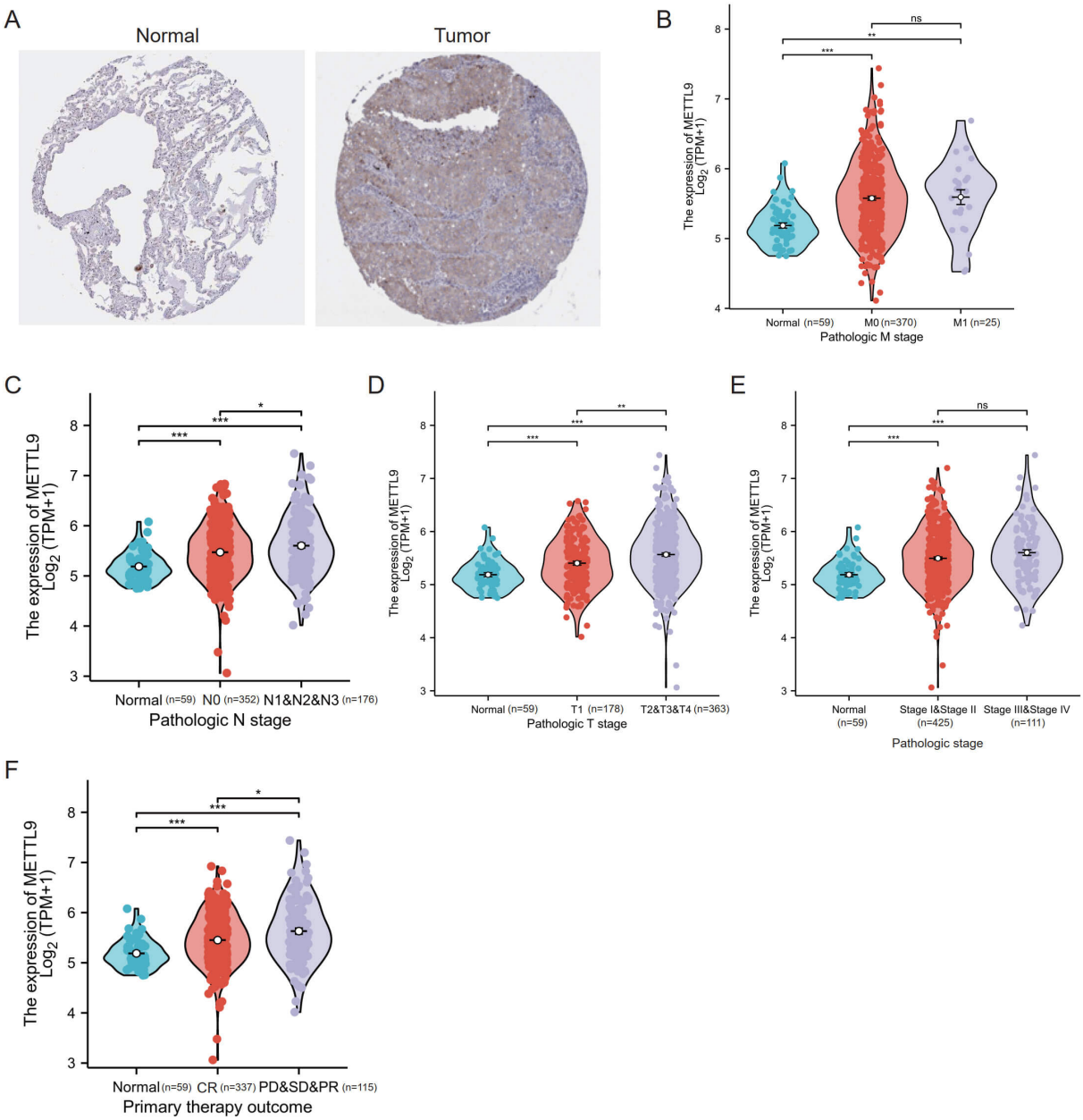

Fig. 2. METTL9 protein expression and association with clinicopathological features. (A) Representative immunohistochemistry (IHC) images of METTL9 expression in LUAD and normal lung tissues were acquired from the Human Protein Atlas (HPA) database (https://www.proteinatlas.org/) with authorization. (B–F) Association of METTL9 protein expression with metastasis stage (M stage), lymph node stage (N stage), tumor stage (T stage), pathological stage, and primary therapy outcome in LUAD based on the Clinical Proteomic Tumor Analysis Consortium (CPTAC) dataset via UALCAN. ns: $p \geq 0.05$; *$p < 0.05$; **$p < 0.01$; ***$p < 0.001$.

comparisons of METTL9 expression, respectively. Associations with clinical features were assessed using Wilcoxon test and logistic regression. Spearman correlation was used for correlation analyses. Data are shown as mean ± SD from at least three independent biological replicates. For comparisons among multiple groups, one-way ANOVA followed by Tukey's post hoc test was performed, while differences between two groups were analyzed using the *t*-test. Differences with $p < 0.05$ were considered statistically significant.

3. Results

3.1 METTL9 Is Slightly but Significantly Upregulated in LUAD

Pancancer analysis revealed that METTL9 expression was dysregulated across multiple tumor types (Fig. 1A). In LUAD, tumor tissues exhibited modestly but significantly greater METTL9 expression than normal lung tissues (Fig. 1B), with mean TPM values of 5.51 in tumors vs. 5.19 in normal tissues, corresponding to a Fold Change (FC) of 1.06 (log2FC = 0.088). Consistently, paired anal-

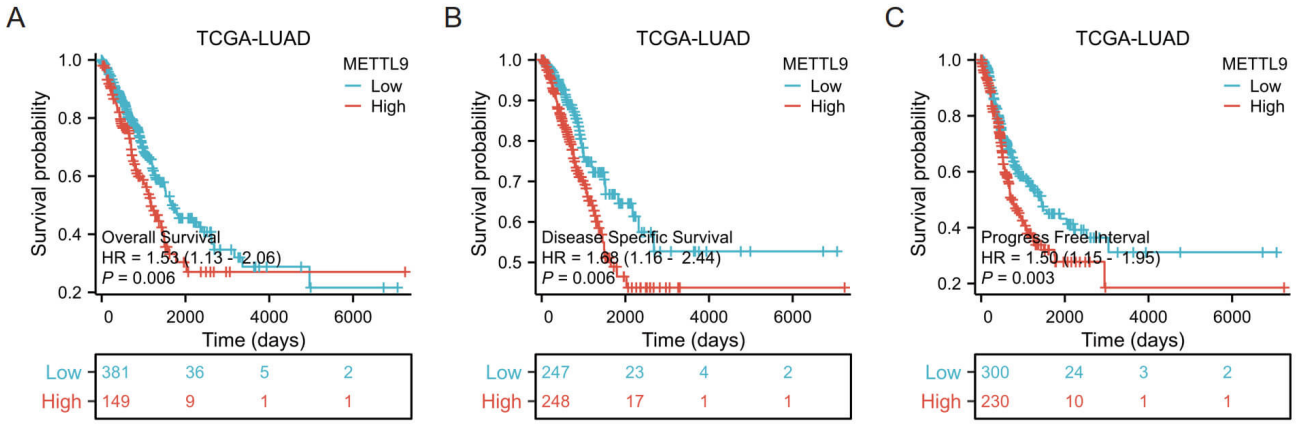

Fig. 3. Association of METTL9 expression with prognosis in LUAD. (A–C) Kaplan–Meier survival curves for (A) overall survival (OS), (B) disease-specific survival (DSS), and (C) progression-free interval (PFI) in TCGA-LUAD cohort.

ysis demonstrated a mild upregulation of METTL9 in tumor tissues versus matched adjacent normal tissues (Fig. 1C), with mean values of 5.67 vs. 5.19, respectively (FC = 1.09, log2FC = 0.127). Notably, although most of the paired samples had higher expression in tumors, the magnitude of increase remained relatively small. External validation using the GSE31210 dataset further confirmed this trend (Fig. 1D), where METTL9 expression was marginally elevated in tumor tissues (mean: 12.16 vs. 11.88 in normal tissues), corresponding to a fold change of 1.02 (log2FC = 0.033). Overall, METTL9 appears to be transcriptionally upregulated in LUAD, but only modestly so, implying that its biological importance may be more related to functional regulation and downstream signaling pathways than to pronounced transcriptional differences. Therefore, subsequent functional experiments were performed to determine whether this modest but consistent upregulation translates to meaningful biological effects on LUAD progression. HPA database–based representative IHC images revealed elevated METTL9 immunostaining in LUAD tissues relative to normal lung tissues (Fig. 2A). However, owing to the limited sample size and lack of biological replicates in the HPA dataset, these findings are considered qualitative and supportive rather than quantitative evidence. These observations were further supported by our in-house IHC analysis, which provided quantitative validation of METTL9 upregulation in LUAD tissues. Furthermore, proteomic analysis of the CPTAC cohort indicated that higher METTL9 protein levels were closely related to advanced pathological stage, tumor progression (T, N, and M), and poor primary therapy outcomes in LUAD (Fig. 2B–F).

3.2 Prognostic and Diagnostic Significance of METTL9 in LUAD

The association between METTL9 expression and prognosis in LUAD was assessed using Kaplan–Meier survival analysis. As illustrated in Fig. 3A, elevated METTL9 expression was linked to significantly reduced OS compared with low expression (hazard ratio [HR] = 1.53; 95% confidence interval [CI]: 1.13–2.06; p = 0.006). In line with these findings, high METTL9 expression was associated with reduced disease-specific survival (DSS) (Fig. 3B) (HR = 1.68; 95% CI: 1.16–2.44; p = 0.006). Moreover, progression-free interval (PFI) analysis showed that increased METTL9 expression correlated with an elevated risk of disease progression (Fig. 3C; HR = 1.50; 95% CI: 1.15–1.95; p = 0.003). Collectively, these results demonstrate a consistent association between elevated METTL9 expression and poor prognosis across multiple survival endpoints in LUAD patients. The diagnostic performance of METTL9 in LUAD was evaluated using Receiver Operating Characteristic (ROC) curve analysis in the TCGA and GSE31210 cohorts (Fig. 4A,B). METTL9 displayed reasonable diagnostic accuracy, with Area Under the Curve (AUC) values of 0.704 (TCGA) and 0.815 (GSE31210), indicating stronger performance in the external validation cohort. To further investigate its clinical relevance, a risk score model based on METTL9 expression was constructed. As presented in Fig. 4C, the high-risk group exhibited earlier endpoint events than the low-risk group, further supporting that high METTL9 expression is associated with poor prognosis. Additionally, the predictive ability of METTL9 for prognosis was evaluated using time-dependent ROC curve analysis. As depicted in Fig. 4D, METTL9 yielded AUC values of 0.526, 0.600, and 0.715 for 3-, 5-, and 10-year survival, respectively. Overall, METTL9 displays limited short-term predictive power but improved accuracy in forecasting long-term survival. Univariate Cox analysis revealed that advanced pathologic stage, higher T/N classification, M1 status, unfavorable primary therapy outcomes (Progressive Disease (PD), Stable Disease (SD), and Partial Response (PR)), and increased METTL9 expression were associated with reduced OS (Fig. 4E). METTL9 was not retained as an independent prognostic variable in the multivariate Cox model (Fig. 4F), sug-

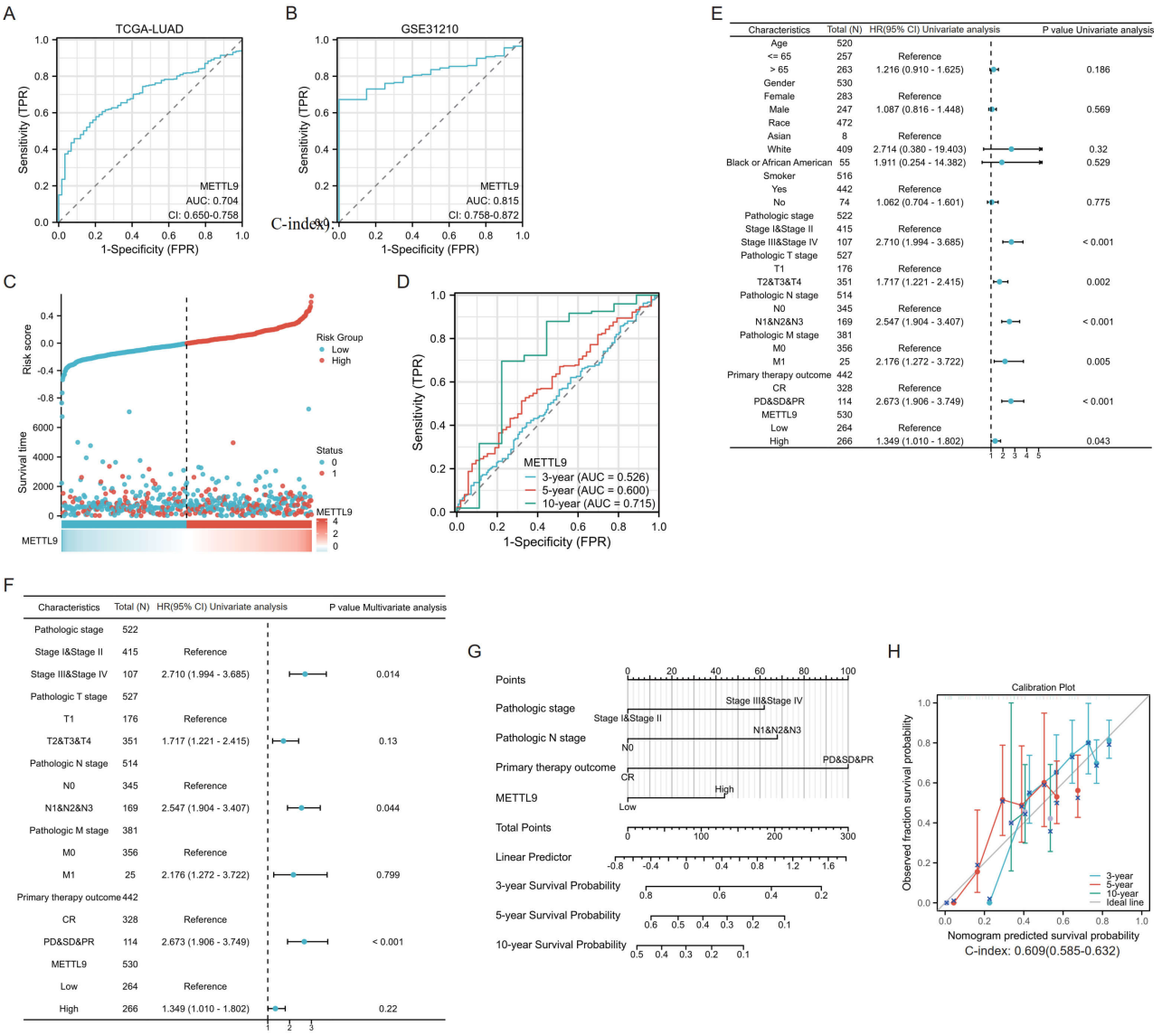

Fig. 4. Predictive value of METTL9 in LUAD. (A,B) Evaluation of METTL9 diagnostic performance based on receiver operating characteristic (ROC) curve analysis in the TCGA and GSE31210 cohorts. (C) Overview of risk scores, survival outcomes, and METTL9 expression heatmap in the TCGA-LUAD dataset. (D) Evaluation of METTL9 for predicting 3-, 5-, and 10-year OS based on time-dependent ROC analysis in the TCGA-LUAD cohort. (E) Forest plot displaying variables associated with OS from univariate Cox regression analysis. (F) Forest plot displaying independent predictors of OS based on multivariate Cox regression analysis. (G) Nomogram predicting 3-, 5-, and 10-year OS. (H) Calibration plot validating the nomogram model.

gesting that its prognostic relevance may be attenuated by more influential clinical parameters, including pathological stage, N stage, and initial treatment outcomes. To predict 3-, 5-, and 10-year survival, a nomogram that included OS-related risk factors (stage, N stage, primary therapeutic outcome, and METTL9 expression) was created. While METTL9 was not an independent predictor in multivariate Cox analysis, it was still included in the model to investigate its potential additional prognostic contribution based on univariate findings (Fig. 4G). According to the calibration curves, METTL9 expression more accurately predicted 5- and 10-year survival than 3-year survival (Fig. 4H).

3.3 DEGs and Enrichment Analysis

Among the high/low-METTL9 groups, 411 DEGs were found (217 upregulated and 194 downregulated) (Fig. 5A). The top 5 upregulated and downregulated genes linked to METTL9 expression are shown in Fig. 5B. Kyoto Encyclopedia of Genes and Genomes (KEGG) analysis identified enrichment of pathways related to taste transduction, mineral absorption, and neuroactive ligand–receptor interaction (Fig. 5C,D). Although some of these pathways, such as taste transduction, may appear unrelated to LUAD at first glance, accumulating evidence suggests that components of these signaling pathways—particularly G protein-

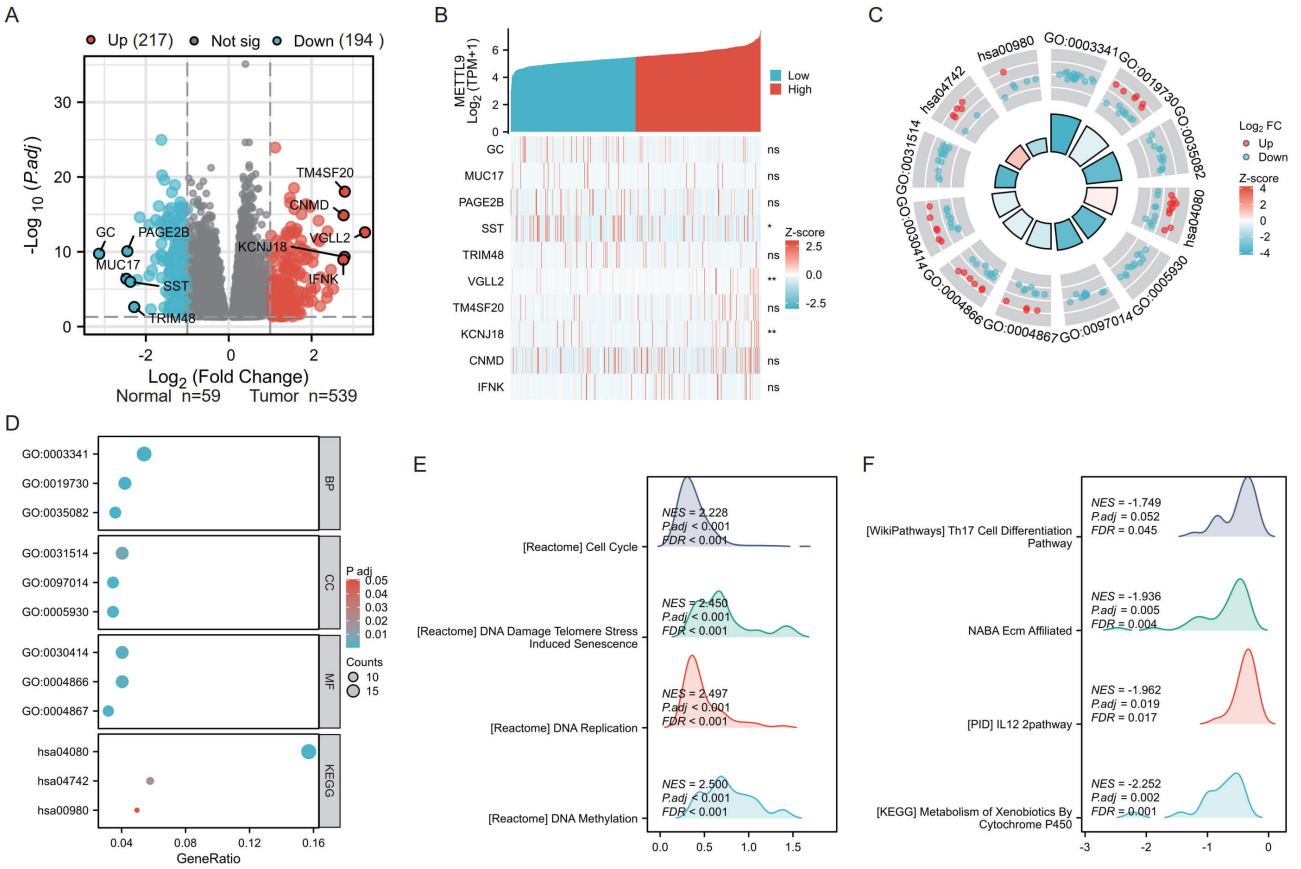

Fig. 5. Differentially expressed genes (DEGs) and functional enrichment associated with METTL9 in LUAD. (A) Volcano plot displaying DEGs associated with high versus low METTL9 expression. (B) Heatmap showing the top five upregulated and downregulated genes in relation to METTL9 expression. (C,D) Bubble and circle plots for Gene Ontology (GO) and Kyoto Encyclopedia of Genes and Genomes (KEGG) enrichment analyses. (E) Gene Set Enrichment Analysis (GSEA) results in samples with high METTL9 abundance. (F) GSEA results in the METTL9 low-expression group. ns: $p \geq 0.05$; *$p < 0.05$; **$p < 0.01$.

coupled receptors (GPCRs) and ion channels—can be aberrantly expressed in cancer cells and contribute to tumor cell proliferation, migration, and signal transduction. Similarly, enrichment in cilium-related processes (e.g., cilium movement and axoneme assembly) may reflect alterations in epithelial cell structure and function. Primary cilia play important roles in cell signaling and maintaining epithelial homeostasis, and their dysfunction has been implicated in tumorigenesis and cancer progression. Therefore, these enrichment results may indicate that METTL9 is involved in regulating epithelial integrity, signaling pathways, and cellular communication in LUAD. According to GSEA, elevated METTL9 expression was associated with pathways related to the cell cycle, DNA damage mechanisms, telomere stress–driven senescence, DNA replication activity, and methylation processes (Fig. 5E,F). These pathways are well-established contributors to tumor progression and thus are more likely to represent biologically meaningful alterations in LUAD than other significantly enriched pathways whose functional relevance may require further validation.

3.4 PPI Network and Cuproptosis-Related Analysis

A PPI network of genes associated with METTL9 was constructed. EEF1AKNMT, IGSF6, METTL18, METTL21C, METTL24, METTL25, METTL2B, METTL7B, METTL8, and OTOA were among the important interacting genes (Fig. 6A). While IGSF6, METTL21C, METTL24, METTL25, and OTOA were downregulated in LUAD, EEF1AKNMT, METTL18, METTL2B, METTL7B, and METTL8 were upregulated (Fig. 6B). The results of the correlation analysis of METTL9 with these genes are shown in Fig. 6C. Gene Ontology (GO) analysis demonstrated significant enrichment in methylation-, methyltransferase activity-, and N-methyltransferase activity-related genes (Fig. 6D). TCGA data analysis demonstrated a significant association between METTL9 expression and multiple cuproptosis-related genes. Moreover, differential expression analysis (Fig. 7A,B) showed significant differences in several cuproptosis-related genes between the high- and low-METTL9 expression groups. However, these findings are based on transcriptomic associations and group compar-

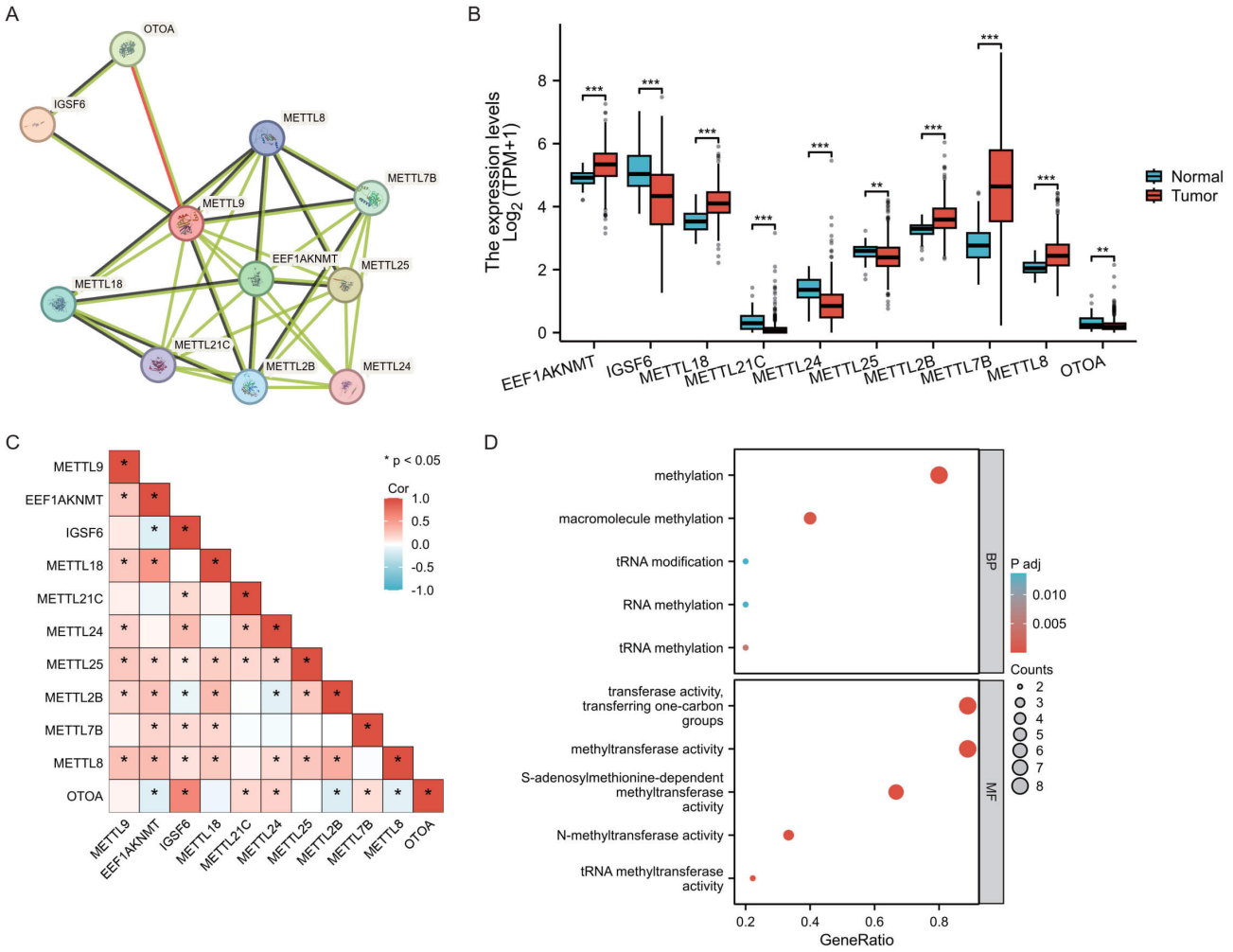

Fig. 6. METTL9-related genes and functional analysis. (A) Protein-protein interaction (PPI) network of METTL9-associated genes. (B) Expression of METTL9-related genes in LUAD. (C) Correlation analysis between METTL9 and related genes. (D) Functional annotation of METTL9-related genes based on GO and KEGG enrichment analysis. *$p < 0.05$; **$p < 0.01$; ***$p < 0.001$.

isons and do not imply a causal regulatory relationship between METTL9 and cuproptosis. Additional functional work is necessary to assess whether METTL9 plays a direct role in regulating cuproptosis in LUAD.

3.5 METTL9 Gene Mutation and DNA Methylation

METTL9 showed missense mutations, splice mutations, amplifications, and deep deletions at a frequency of 1% according to analysis using cBioPortal (Fig. 8A,B). METTL9 mutation status was not strongly correlated with OS or disease-free survival (DFS), as shown by Kaplan–Meier analysis (Fig. 8C,D). Notably, the survival curves exhibited minimal separation, which is likely attributable to the extremely low mutation frequency (~1%) and the resulting small sample size in the mutation subgroup, thereby limiting the statistical power. LUAD tissues have greater METTL9 promoter methylation than normal lung tissues do, according to UALCAN analysis (Fig. 8E).

3.6 METTL9 and Immune Infiltration

TIMER analysis revealed that METTL9 expression correlated with tumor purity (r = 0.091; $p = 0.0436$), B cells (r = −0.09; $p = 0.0481$), $CD8^+$ T cells (r = 0.189; $p = 2.62 \times 10^{-5}$), $CD4^+$ T cells (r = −0.129; $p = 0.00439$), macrophages (r = 0.149; $p = 0.001$), neutrophils (r = 0.195; $p = 1.52 \times 10^{-5}$), and dendritic cells (DCs; r = 0.129; $p = 0.00443$) in LUAD (Fig. 9A). ssGSEA revealed that METTL9 was positively associated with T helper 2 (Th2) cells, Gamma-delta T (γδ T)(Tgd) cells, and neutrophils but negatively correlated with Tregs, NK cells, T cells, $CD8^+$ T cells, Tfh cells, effector memory T (Tem) cells, B cells, cytotoxic cells, natural killer CD56bright (NK CD56bright) cells, T helper 17 (Th17) cells, and plasmacytoid DCs (Fig. 9B–N). METTL9 expression correlated positively with KRAS and negatively with PDCD1 in LUAD (Fig. 9O,P).

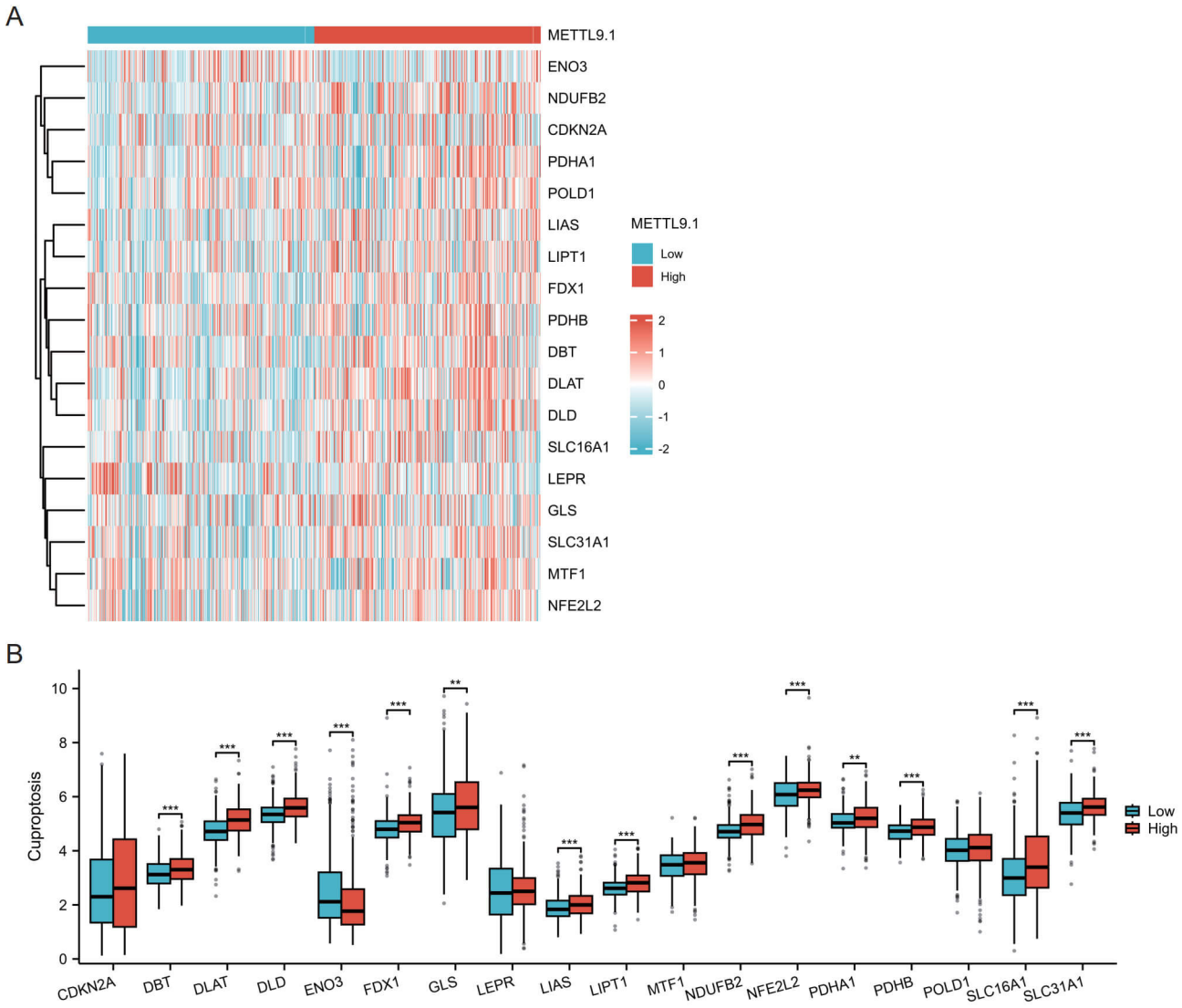

Fig. 7. Correlation between METTL9 and cuproptosis-related genes. (A) Correlation heatmap of METTL9 and cuproptosis-related genes. (B) Expression of cuproptosis-related genes in METTL9 high-expression and low-expression groups. $^{**}p < 0.01$; $^{***}p < 0.001$.

3.7 Validation of METTL9 Expression and Function in LUAD Cells

High METTL9 expression in LUAD was confirmed by IHC staining of ten paired LUAD and adjacent non-cancerous tissue samples (Fig. 10A,B). Compared with that in BEAS-2B and IMR90 cells, METTL9 expression was greatly elevated in A549 and H1975 cells (Fig. 10C). In A549 and H1975 cells, shRNA (sh-METTL9#1, sh-METTL9#2, and sh-METTL9#3) strongly decreased METTL9 mRNA levels (Fig. 10D–H). For later tests, sh-METTL9#2 and sh-METTL9#3 were utilized. The results of functional tests revealed that METTL9 knockdown decreased cell viability (Fig. 11A,B), proliferation (Fig. 11C–E), migration (Fig. 11F–H), and invasion (Fig. 11I–K). METTL9 depletion increased apoptosis, reduced Bcl-2 expression (Fig. 12A–F) and decreased p-smad2 and p-smad3 levels (Fig. 12D,G–J). Additionally, METTL9 knockdown impeded EMT by repressing N-cadherin and vimentin expression while increasing E-cadherin and β-catenin expression (Fig. 13A–I).

4. Discussion

The level and functional role of METTL9 in LUAD were methodically described in this investigation. METTL9 expression is consistently increased in LUAD tissues, according to our studies. Increased METTL9 expression was linked to advanced tumor stage, poor primary therapy outcomes, and reduced OS. Interestingly, although METTL9 exhibited increased promoter methylation in LUAD, its expression was simultaneously upregulated. This apparent discrepancy indicates that promoter methylation alone may not fully account for the regulation of METTL9 expression. In certain situations, methylation at specific CpG sites or regions does not necessar-

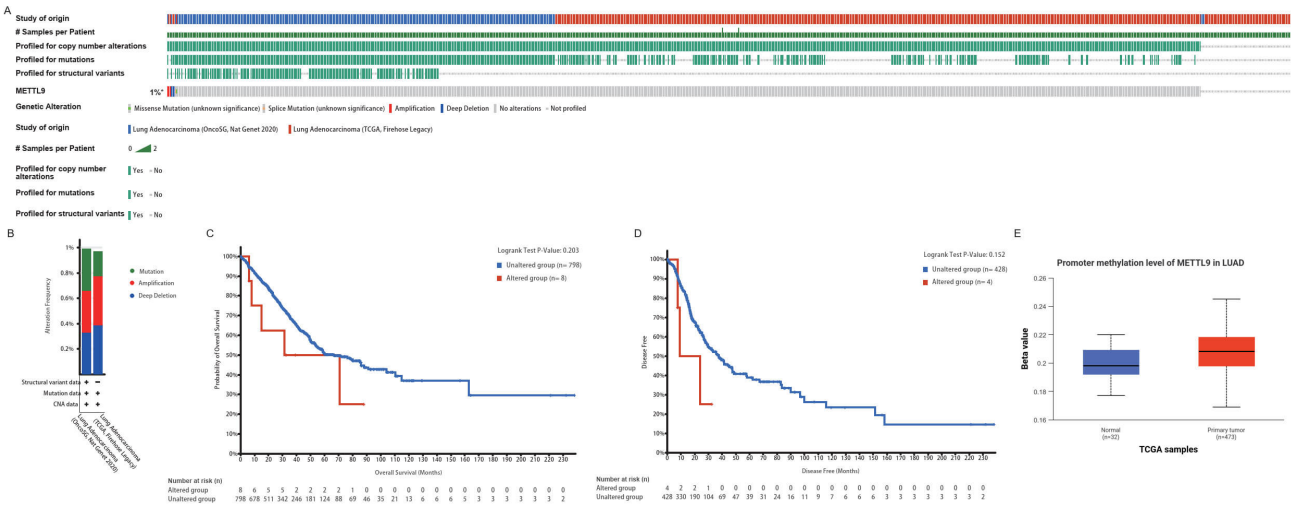

Fig. 8. METTL9 mutation and DNA methylation and their impact on LUAD prognosis. (A,B) METTL9 mutation profile in cBioPortal OncoPrint. (C) Association between METTL9 mutation and OS in LUAD. (D) Association between METTL9 mutation and disease-free survival (DFS) in LUAD. (E) METTL9 promoter methylation levels in LUAD from the UALCAN database.

ily suppress transcription, especially when additional regulatory mechanisms—such as enhancer activity, transcription factor binding, or posttranscriptional modifications—are involved. Therefore, the concurrent occurrence of elevated promoter methylation and increased METTL9 expression may reflect the interplay of multiple regulatory layers. While previous studies on METTL family proteins, such as METTL3 and METTL14, have focused predominantly on m6A-mediated regulation of RNA stability and translation in various cancers, METTL9 has not been extensively studied in the context of LUAD. For instance, in breast cancer, the METTL3/IGF2BP3 axis drives m6A alterations in Programmed Death-Ligand 1 (PD-L1) mRNA, preventing tumor immune surveillance [18]. Additionally, METTL3 promotes colorectal cancer lung metastasis through the recruitment of M2-type immunosuppressive macrophages via m6A-SNAIL [19]. Target recognition of m6A modification is affected by the METTL14 R298P mutation, which disrupts gene expression patterns and cell growth [20]. Furthermore, METTL14 promotes sorafenib-induced ferroptosis in cervical carcinoma by decreasing the stability of Ferritin Heavy Chain 1 (FTH1) mRNA via m6A methylation [21]. Our study demonstrated that high METTL9 expression is associated with poor prognosis in patients with LUAD, as indicated by the univariate analysis. However, multivariate Cox analysis did not identify METTL9 as an independent prognostic factor, suggesting that its prognostic effect may be influenced or confounded by stronger clinical variables such as tumor stage, N stage, or treatment outcomes. Consequently, METTL9 may function as a supplementary prognostic indicator rather than a standalone predictor. Nonetheless, its biological role and potential as a therapeutic target merit further investigation. Enrichment analysis revealed pathways including taste transduction and cilium-related processes. Although these pathways are not conventionally linked to lung cancer, emerging evidence shows that taste receptors and associated GPCR signaling components can be ectopically expressed in various tumors, potentially influencing cell proliferation and migration [22]. Similarly, cilia-related processes are crucial for epithelial cell differentiation and signal transduction, and their dysregulation has been implicated in tumorigenesis [23]. These observations support a potential role of METTL9 in LUAD progression, potentially through its effects on nonclassical signaling pathways and epithelial structural dynamics. It is essential to distinguish between statistical significance and biological relevance in enrichment analyses. While multiple pathways reached statistical significance on the basis of the FDR thresholds, not all of these pathways may play direct roles in LUAD progression. Significant enrichment primarily reflects coordinated changes in gene expression rather than causative or functionally relevant effects. Therefore, we focused on pathways with established roles in cancer, such as cell cycle regulation, DNA replication, and EMT-related signaling, which are biologically meaningful. Other enriched pathways may represent indirect effects or tissue-specific characteristics, and further experimental validation is needed to confirm their functional significance.

Functionally, METTL9 knockdown in A549 and H1975 cells led to decreased proliferation, migration, invasion, and EMT and increased apoptosis. These findings align with studies showing that other METTL family members promote tumor progression [24,25], although the precise molecular mechanisms underlying METTL9 function in LUAD remain unclear. Given the reported roles of METTL9 in regulating mitochondria-associated proteins, including the methylation of the Ubiquinone Oxidoreduc-

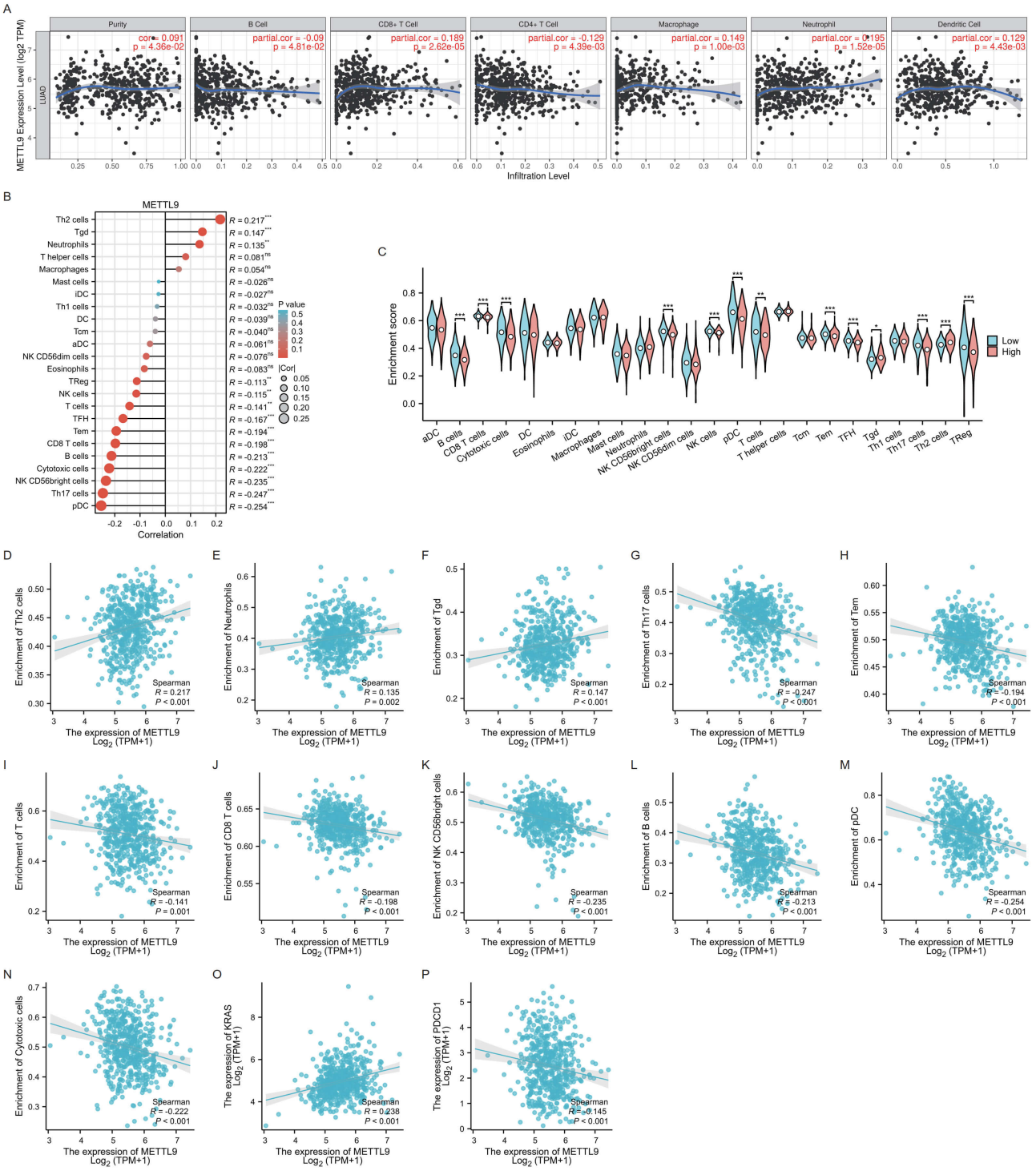

Fig. 9. Correlation of METTL9 expression with immune infiltration, oncogene and immune checkpoints. (A) Association between METTL9 expression level and immune infiltration for purity, B cell, CD8+ T cell, CD4+ T cell, macrophage, neutrophil and dendritic cell based on analyses from the Tumor Immune Estimation Resource (TIMER) database. (B) Bubble plot showing correlations between METTL9 and 24 types of immune cells estimated by the ssGSEA algorithm. (C) Immune cell infiltration profiles compared between high- and low-METTL9 activity groups. (D–N) Scatter plots analysis of relationships between METTL9 levels and T helper 2 (Th2) cells, neutrophils, gamma delta T cells (γδ T cells, Tgd), T helper 17 (Th17) cells, effector memory T cells (Tem), total T cells, $CD8^+$ cytotoxic T cells, natural killer CD56bright (NK CD56bright) cells, B cells, plasmacytoid dendritic cells (pDCs), and cytotoxic cells. (O,P) Scatter plots showing correlations between METTL9 expression and Kirsten rat sarcoma viral oncogene homolog (KRAS) and programmed cell death protein 1 (PDCD1). ns: $p \geq 0.05$; *$p < 0.05$; **$p < 0.01$; ***$p < 0.001$.

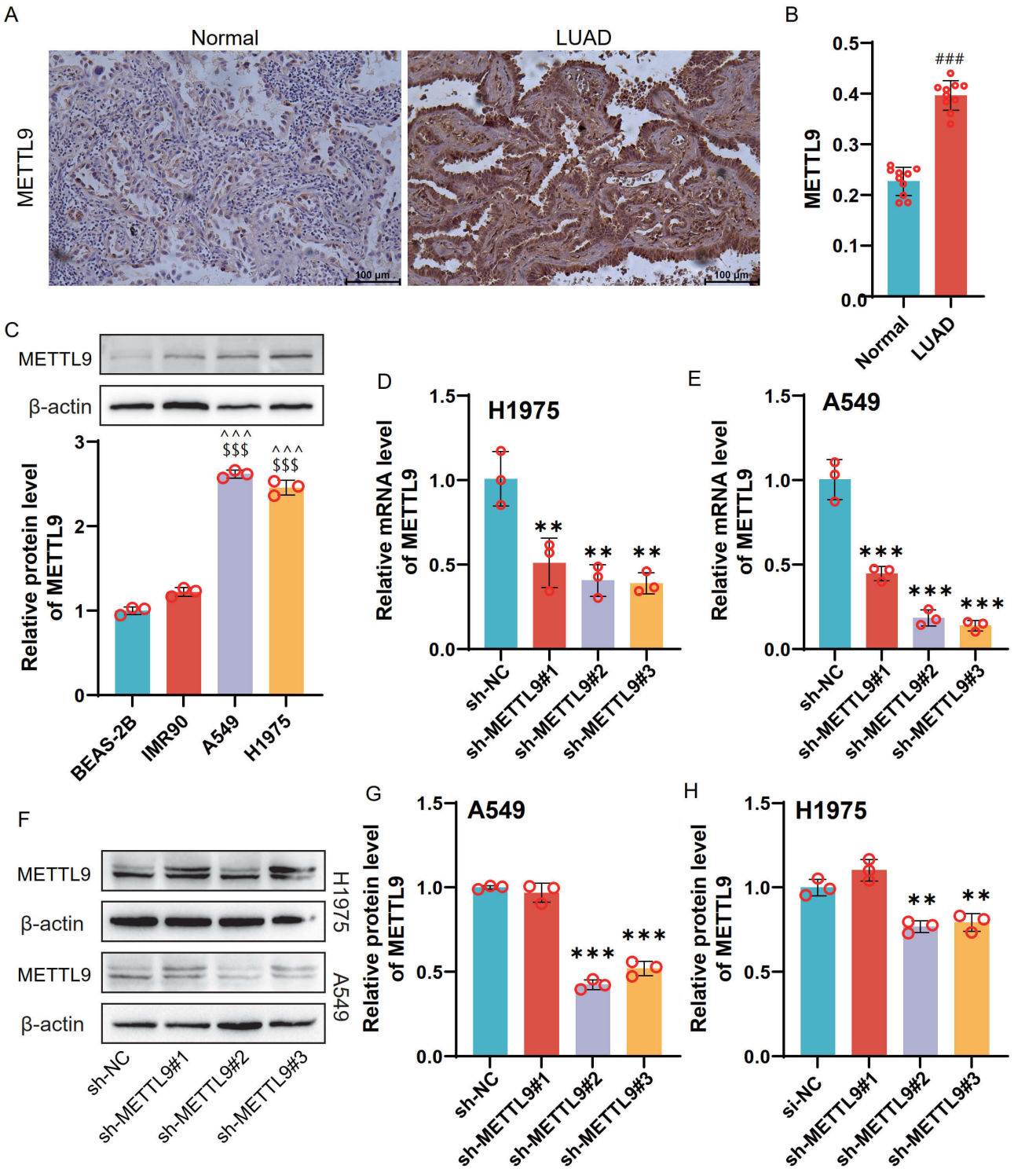

Fig. 10. METTL9 expression in clinical samples and LUAD cell lines. (A,B) Representative Immunohistochemistry (IHC) images of METTL9 in 10 LUAD samples and adjacent non-tumorous lung tissues. Scale bar = 100 μm. (C) Western blot evaluation of METTL9 in BEAS-2B human bronchial epithelial cells, IMR90 human fetal lung fibroblasts, and LUAD cell lines A549 and H1975. (D,E) Reverse transcription-quantitative polymerase chain reaction (RT-qPCR) analysis of METTL9 expression in METTL9 knockdown and control A549 and H1975 cell lines. (F–H) Western blot evaluation of METTL9 in the corresponding groups. All experiments were performed with at least three independent biological replicates. Data are presented as mean ± SD. $^{###}p < 0.01$ vs. normal; $^{\wedge\wedge\wedge}p < 0.001$ vs. BEAS-2B; $^{\$\$\$}p < 0.001$ vs. IMR90; $^{**}p < 0.01$, $^{***}p < 0.001$ vs. sh-NC.

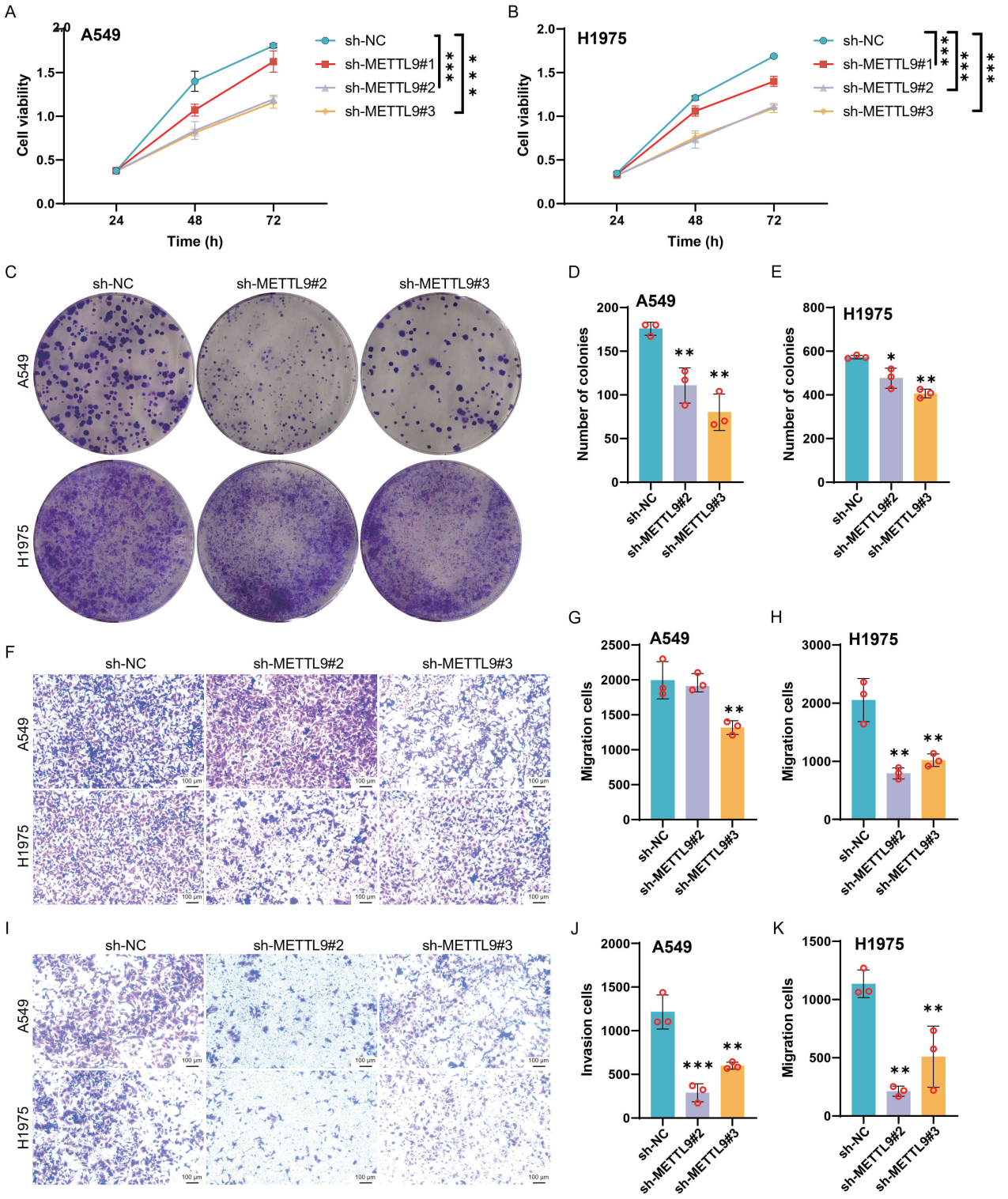

Fig. 11. Effect of METTL9 knockdown on LUAD cell proliferation, migration, and invasion. (A,B) Cell Counting Kit-8 (CCK8) assay of A549 and H1975 cells in the presence or absence of METTL9 knockdown. (C–E) Colony formation assay of A549 and H1975 cells in the presence or absence of METTL9 knockdown. (F–K) Migration and invasion of A549 and H1975 cells assessed by Transwell assays in the presence or absence of METTL9 knockdown. Scale bar = 100 µm. All assays were carried out with at least three independent biological replicates. Data are presented as mean ± SD. *$p < 0.05$; **$p < 0.01$; ***$p < 0.001$ vs. sh-NC.

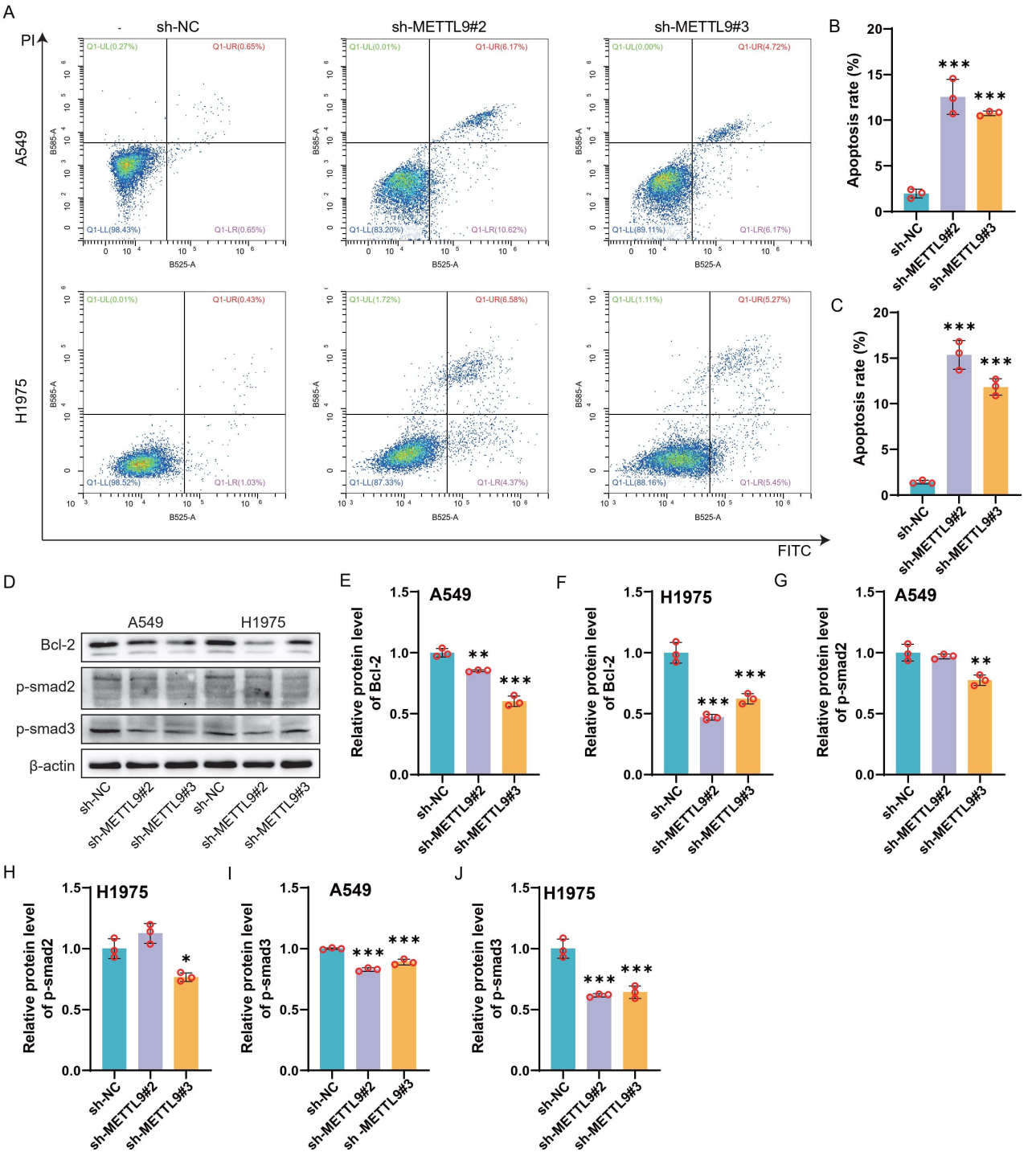

Fig. 12. Effect of METTL9 knockdown on apoptosis and TGF-β/Smad signaling in LUAD cells. (A–C) Flow cytometry–based apoptosis assessment in A549 and H1975 cells in the presence or absence of METTL9 knockdown. (D–J) Protein expression of B-cell lymphoma 2 (Bcl-2), phosphorylated mothers against decapentaplegic homolog 2 (p-Smad2), and phosphorylated Smad3 (p-Smad3) was evaluated by Western blot in A549 and H1975 cells following METTL9 knockdown. All assays were carried out with at least three independent biological replicates. Data are presented as mean ± SD. *$p < 0.05$; **$p < 0.01$; ***$p < 0.001$ vs. sh-NC.

tase Subunit B3 (NDUFB3) subunit of mitochondrial respiratory complex I and the enhancement of complex I-mediated respiration, depletion of METTL9 may impair mitochondrial activity. Such impairment could disrupt cellular energy homeostasis, contributing to reduced proliferative capacity and increased apoptosis [26]. Moreover, our data indicate that METTL9 knockdown is associated with reduced activity of the TGF-β/Smad signaling cascade, sug-

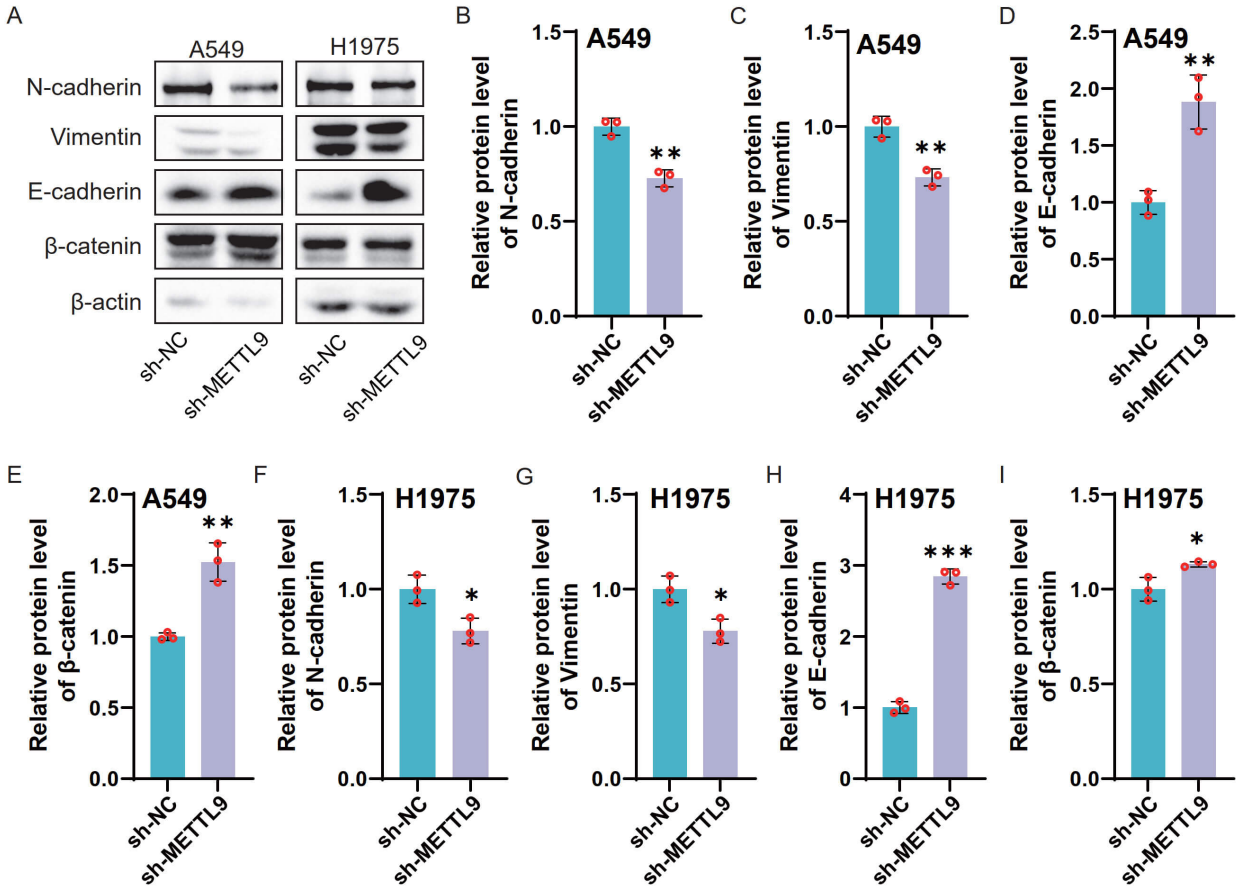

Fig. 13. Effect of METTL9 knockdown on epithelial-mesenchymal transition (EMT) markers in LUAD cells. (A–I) Western blot evaluation of N-cadherin, vimentin, E-cadherin, and β-catenin in A549 and H1975 cells with METTL9 knockdown. All assays were carried out with at least three independent biological replicates. Data are presented as mean ± SD. *$p < 0.05$; **$p < 0.01$; ***$p < 0.001$ vs. sh-NC.

gesting a potential link between METTL9 and proliferation-related signaling networks. However, whether this pathway directly mediates the antiproliferative effects of METTL9 depletion remains unclear, and it is also possible that the observed phenotypes result from broader alterations in cellular metabolic or transcriptional programs rather than a single signaling axis. In addition, although our study showed that METTL9 depletion on proliferation and apoptosis, we did not directly investigate several potential downstream targets, such as S100A9 and mitochondrial complex subunits. S100A9 has been shown to play important roles in inflammatory processes and tumor progression [27], whereas mitochondrial complex subunits are essential for cellular energy metabolism [28]. METTL9 may influence these targets, thereby contributing to the observed phenotypes. Future studies are warranted to determine whether METTL9 directly regulates S100A9 expression or mitochondrial complex assembly, which would provide further insight into the molecular mechanisms underlying its function in LUAD. According to earlier research, Dual-Specificity Phosphatase 5 (DUSP5) uses TGF-β/SMAD to induce epithelial–mesenchymal transition and Epidermal Growth Factor Receptor–Tyrosine Kinase Inhibitor (EGFR-TKI) resistance in lung cancer [29]. Proteasome Activator Subunit 3 (PSME3) has been shown to facilitate the development of LUAD through regulation of TGF-β/Smad [30]. Additionally, the downregulation of manifold glycosyltransferase (MFNG) expression was reported to increase the metastatic potential of LUAD through the modulation of TGF-β/SMAD activity [31]. In addition to expression and functional analyses, we examined the mutation profile of METTL9 in LUAD. Notably, METTL9 mutations were rare (~1%), limiting the statistical power to detect associations with clinical outcomes and potentially explaining the minimal separation observed in survival curves between the mutation and wild-type groups. Thus, the biological significance of METTL9 mutations in LUAD remains uncertain and warrants validation in larger cohorts. Our analysis also revealed a potential link between METTL9 expression and immune infiltration patterns in LUAD. However, these observations are primarily based on bioinformatics inference rather than direct experimental evidence. Accumulating evidence suggests that epigenetic regulators can regulate the tumor immune microen-

vironment through effects on immune cell recruitment and activation [32,33]. Therefore, METTL9 may participate in immune-related regulatory processes, but this hypothesis requires functional validation through assays such as coculture systems or *in vivo* models. Importantly, our study provides initial evidence linking METTL9 to TGF-β/Smad signaling, as reflected by the reduced phosphorylation levels of Smad2 and Smad3 following METTL9 knockdown. Nevertheless, these results are derived from loss-of-function experiments and do not establish a direct regulatory relationship. In the absence of upstream mechanistic studies or rescue experiments, whether METTL9 directly regulates TGF-β/Smad signaling or acts indirectly remains unclear. Given that METTL9 is a histidine methyltransferase with specificity for histone motifs [23], the observed suppression of the TGF-β/Smad pathway may result from methylation of an as-yet-unidentified regulatory protein. Whether METTL9 directly affects signaling receptors or Smad proteins or whether this effect is a secondary consequence of broader epigenetic modifications remains unknown. Future studies, including chromatin immunoprecipitation and identification of direct methylation targets, are needed to elucidate how METTL9 modulates TGF-β/Smad signaling in LUAD cells.

A newly identified type of planned cell death is called cuproptosis [34,35]. Previous studies have demonstrated that the Spleen Focus Forming Virus (SFFV) Proviral Integration Oncogene/ Cyclin-Dependent Kinase Inhibitor 2A/ Tumor Protein p53 (SPI1/CDKN2A/p53) axis regulates LUAD cell proliferation, migration, and drug sensitivity via cuproptosis [36]. Other studies have shown that 4-octyl itaconate promotes cuproptosis in colorectal cancer by targeting GAPDH [37] and that knockdown of Ferredoxin 1 inhibits colorectal cancer progression and regulates cuproptosis via the Hippo signaling pathway [38]. To explore the potential links between METTL9 and novel cell death pathways, we evaluated the correlation between METTL9 expression and 18 cuproptosis-related genes. TCGA data demonstrated that METTL9 expression was positively correlated with several cuproptosis regulators such as Dihydrolipoamide Branched Chain Transacylase E2 (DBT), Dihydrolipoamide S-Acetyltransferase (DLAT), and Ferredoxin 1 (FDX1), but a negative correlation with Enolase 3 (ENO3) expression. These results indicate a possible transcriptional relationship linking METTL9 with components of the cuproptosis machinery, which warrants further investigation. Therefore, the proposed link between METTL9 and cuproptosis should be viewed as preliminary and hypothesis-generating. Additional experimental studies are required to clarify whether METTL9 directly affects cuproptosis and to elucidate the underlying molecular mechanisms.

Finally, our research revealed that different immune cell types are linked to METTL9 expression. METTL9 expression was negatively associated with the levels of cytotoxic and adaptive immune cells, such as $CD8^+$ T cells, NK cells, B cells, and Th17 cells, but tended to increase in the presence of Th2 cells, Tgd cells, and neutrophils. Previous studies have shown that fascin actin-bundling protein 1 (FSCN1)-induced protein tyrosine phosphatase receptor type F (PTPRF)-dependent inflammatory reprogramming of the TME promotes LUAD progression by regulating macrophage glycolysis [39]. In LUAD, tumor-derived Immunoglobulin Like Transcript 3 (ILT3) increases the effectiveness of PD-L1 inhibition and inhibits the remodeling of an immunosuppressive milieu [40]. In addition, serine/threonine kinase 24 (STK24) promotes LUAD progression while modulating the immune microenvironment [41]. This pattern suggests that high METTL9 expression contributes to a tumor microenvironment conducive to LUAD progression. By supporting protumor immune populations and suppressing antitumor effector cells, METTL9 may facilitate immune evasion, tumor growth, and metastasis. Moreover, METTL9 expression showed a negative correlation with PDCD and a positive correlation with KRAS. An important immunological checkpoint that controls T-cell activity is PD-1 [42,43], and its downregulation in the context of high METTL9 expression may reflect an immunosuppressive microenvironment that limits effective cytotoxic T-cell responses. Because this observation is based on a transcriptomic correlation analysis, a direct regulatory or mechanistic link between METTL9 and PD-1-related immune pathways in LUAD was not established. Accordingly, additional experimental studies are required to clarify whether METTL9 functionally modulates these immune pathways. In addition, alternative explanations should be considered. METTL9 may be coexpressed with genes involved in cell proliferation, and highly proliferative tumors are often accompanied by reduced immune cell infiltration and altered immune microenvironments. This proliferation-associated immune exclusion may partially explain the observed relationship of METTL9 expression with immune-related features. Accordingly, METTL9 expression in LUAD may not necessarily indicate a direct role in regulating immune infiltration. Instead, it could represent an indirect association driven by proliferation-related transcriptional programs. Additional studies are needed to clarify whether METTL9 directly influences tumor immunity or primarily serves as a marker of proliferative, immune-evasive tumor states. KRAS is a well-known oncogene that is frequently mutated in LUAD, driving tumor proliferation, survival, and metastasis [44,45]. The positive association between METTL9 and KRAS suggests that METTL9 may cooperate with oncogenic signaling to increase tumor aggressiveness.

Overall, our study extends previous findings on METTL family proteins by identifying METTL9 as a critical regulator of LUAD proliferation, EMT, cuproptosis, and immune interactions. Compared with prior studies that emphasized the general oncogenic roles of METTLs, we pro-

vide specific mechanistic insights into LUAD and reveal novel links to cuproptosis and TME modulation.

5. Limitations

This study has several limitations. Notably, although METTL9 protein expression was validated by IHC in LUAD tissues, its relationship with immune infiltration was not directly confirmed. Future studies using multiplex IHC or flow cytometry are needed to validate correlations with specific immune cell populations. Second, the PPI network and cuproptosis-related analyses were based on bioinformatic correlations and remain exploratory. Functional experiments in which METTL9 is manipulated and cuproptotic cell death is assessed are necessary to establish causality. Third, METTL9 mutations occur at a low frequency (~1%), limiting statistical power and the ability to draw definitive conclusions regarding clinical relevance. Fourth, functional assays primarily relied on METTL9 knockdown. While knockdown suppressed tumor cell proliferation, migration, invasion, and EMT, and enhanced apoptosis, complementary overexpression or rescue experiments were not performed. Consequently, the causal relationship between METTL9 and these phenotypes remains unconfirmed. Similarly, although METTL9 knockdown reduced Smad2/3 phosphorylation, the mechanistic link to TGF-β/Smad signaling requires validation through pathway-specific activation, inhibition, or rescue assays. Fifth, EMT inhibition was inferred from marker expression without direct morphological confirmation or *in vivo* validation. The specific methylation targets of METTL9 were not identified, and Smad reporter assays were not conducted; thus, the proposed mechanistic pathways were indirect. Finally, *in vivo* experiments were lacking, and only two LUAD cell lines (A549 and H1975) were used, potentially limiting the generalizability of the findings. Future studies using additional cell lines, patient-derived models, and animal models are warranted to confirm the biological and therapeutic relevance of METTL9 in LUAD.

6. Conclusion

In summary, our integrative analysis combining multiomics datasets, clinical validation, and functional experiments demonstrated that METTL9 is consistently overexpressed in LUAD and correlates with advanced tumor stage and unfavorable prognosis. Functional assays showed that METTL9 enhances LUAD cell proliferation, migration, invasion, and epithelial–mesenchymal transition, potentially via regulation of the TGF-β/Smad signaling pathway. Bioinformatic analyses further revealed associations between METTL9 expression, cuproptosis-related gene expression, and immune cell infiltration patterns, highlighting its potential involvement in tumor metabolism and the tumor microenvironment.

Availability of Data and Materials

The datasets analyzed in this study are publicly available. Transcriptomic and clinical data for lung adenocarcinoma (LUAD) were obtained from The Cancer Genome Atlas (TCGA) database (https://portal.gdc.cancer.gov/) and normal tissue data were obtained from the Genotype-Tissue Expression (GTEx) project (https://gtexportal.org/). The external validation dataset GSE31210 was downloaded from the Gene Expression Omnibus (GEO) database (https://www.ncbi.nlm.nih.gov/geo/). Protein expression data were obtained from the Clinical Proteomic Tumor Analysis Consortium (CPTAC) through the UALCAN portal (https://ualcan.path.uab.edu/analysis-prot.html). Immunohistochemistry (IHC) data were obtained from the Human Protein Atlas (HPA) database (https://www.proteinatlas.org/). Some images used in this study were downloaded from public databases with permission, including images from the Human Protein Atlas (HPA) database. All databases used in this study provide publicly accessible data for research purposes. All research data supporting the findings of this investigation can be obtained by contacting the corresponding author with a justified request.

Author Contributions

CG and YC contributed equally to this work. CG and XZ conceived and designed the study. YC, YX, and YL performed the bioinformatics analysis and data interpretation. LJ and HJ conducted the *in vitro* experiments. ZC and BY assisted with data collection and statistical analysis. YX, YLL, LJ, and HYJ wrote the initial draft. XZ supervised the project and revised the manuscript. All authors contributed to editorial changes in the manuscript. All authors reviewed and approved the final manuscript. All authors have participated sufficiently in the work and agreed to be accountable for all aspects of the work.

Ethics Approval and Consent to Participate

This study was approved by the Ethical Committee of Suzhou Hospital of Anhui Medical University (KY-YJ-2025-014). Written informed consent was obtained from all participants in accordance with the Declaration of Helsinki.

Acknowledgment

Not applicable.

Funding

This study was funded by 2023 Anhui Provincial Health Science and Technology Project (AHWJ2023A30205, Applicant: Chen Gong), 2024 Anhui Provincial Health Science and Technology Project (2024BAd20017, Applicant: Xueqin Zhang), 2023 Suzhou City Science and Technology Plan Project (SZKJXM202428, Applicant: Xueqin Zhang), 2023 Suzhou City Health Science and Technology Project

(SZWJ2023a001, Applicant: Chen Gong), 2023 Anhui Medical University Scientific Research Project (2023xkj075, Applicant: Chen Gong), 2021 Suzhou City Science and Technology Plan Project (SZSKJJZC030, Applicant: Yuyan Chen).

Conflicts of Interest

The authors declare no conflicts of interest.

Supplementary Material

Supplementary material associated with this article can be found, in the online version, at https://doi.org/10.31083/FBL49673.

References

[1] Seguin L, Durandy M, Feral CC. Lung Adenocarcinoma Tumor Origin: A Guide for Personalized Medicine. Cancers. 2022; 14: 1759. https://doi.org/10.3390/cancers14071759

[2] Lahiri A, Maji A, Potdar PD, Singh N, Parikh P, Bisht B, et al. Lung cancer immunotherapy: progress, pitfalls, and promises. Molecular Cancer. 2023; 22: 40. https://doi.org/10.1186/s12943-023-01740-y

[3] Li J, Wang Y, Liu Y, Liu Q, Shen H, Ren X, et al. Survival analysis and clinicopathological features of patients with stage IA lung adenocarcinoma. Heliyon. 2024; 10: e23205. https://doi.org/10.1016/j.heliyon.2023.e23205

[4] Wang Q, Xue F, Assaraf YG, Lin Y. Harnessing Natural Products to Surmount Drug Resistance in Gastric Cancer: Mechanisms and Therapeutic Perspectives. International Journal of Biological Sciences. 2025; 21: 4604–4628. https://doi.org/10.7150/ijbs.113709

[5] Qi YN, Liu Z, Hong LL, Li P, Ling ZQ. Methyltransferase-like proteins in cancer biology and potential therapeutic targeting. Journal of Hematology & Oncology. 2023; 16: 89. https://doi.org/10.1186/s13045-023-01477-7

[6] Wu S, Guo D, Hu X, Yang M. The methyltransferase-like proteins as core regulators of nucleic acid modifications and post-translation modification of proteins in disease pathogenesis and therapeutic implications. Biomarker Research. 2025; 13: 141. https://doi.org/10.1186/s40364-025-00858-z

[7] Sun Y, Shen W, Hu S, Lyu Q, Wang Q, Wei T, et al. METTL3 promotes chemoresistance in small cell lung cancer by inducing mitophagy. Journal of Experimental & Clinical Cancer Research : CR. 2023; 42: 65. https://doi.org/10.1186/s13046-023-02638-9

[8] Sun Y, Gong W, Zhang S. METTL3 promotes colorectal cancer progression through activating JAK1/STAT3 signaling pathway. Cell Death & Disease. 2023; 14: 765. https://doi.org/10.1038/s41419-023-06287-w

[9] Kang N, Zhao Z, Wang Z, Ning J, Wang H, Zhang W, et al. METTL3 regulates thyroid cancer differentiation and chemosensitivity by modulating PAX8. International Journal of Biological Sciences. 2024; 20: 3426–3441. https://doi.org/10.7150/ijbs.84797

[10] Zhang P, Xiang H, Peng Q, Ma L, Weng C, Liu G, et al. METTL14 attenuates cancer stemness by suppressing ATF5/WDR74/β-catenin axis in gastric cancer. Cancer Science. 2025; 116: 112–127. https://doi.org/10.1111/cas.16381

[11] Hou Y, Zhang X, Yao H, Hou L, Zhang Q, Tao E, et al. METTL14 modulates glycolysis to inhibit colorectal tumorigenesis in p53-wild-type cells. EMBO Reports. 2023; 24: e56325. https://doi.org/10.15252/embr.202256325

[12] Codino A, Spagnoletti L, Olobardi C, Cuomo A, Santos-Rosa H, Palomba M, et al. METTL9 sustains vertebrate neural development primarily via non-catalytic functions. Nature Communications. 2025; 16: 7051. https://doi.org/10.1038/s41467-025-62414-5

[13] Jin J, Li Q, Zhang Y, Ji P, Wang X, Zhang Y, et al. METTL9 mediated N1-Histidine methylation of SLC39A7 confers ferroptosis resistance and inhibits adipogenic differentiation in mesenchymal stem cells. Molecular Medicine (Cambridge, Mass.). 2025; 31: 206. https://doi.org/10.1186/s10020-025-01271-w

[14] Li M, Zhi Z, Jiang X, Duan GC, Zhu WN, Pang Z, et al. METTL9 derived circular RNA circ-METTL9 sponges miR-551b-5p to accelerate colorectal cancer progression by upregulating CDK6. Carcinogenesis. 2023; 44: 463–475. https://doi.org/10.1093/carcin/bgad031

[15] Bi F, Qiu Y, Wu Z, Liu S, Zuo D, Huang Z, et al. METTL9-SLC7A11 axis promotes hepatocellular carcinoma progression through ferroptosis inhibition. Cell Death Discovery. 2023; 9: 428. https://doi.org/10.1038/s41420-023-01723-4

[16] Stagg J. Immune regulation by mesenchymal stem cells: two sides to the coin. Tissue Antigens. 2007; 69: 1–9. https://doi.org/10.1111/j.1399-0039.2006.00739.x

[17] Srinivasan D, Balakrishnan R, Chauhan A, Kumar J, Girija DM, Shrestha R, et al. Epithelial-Mesenchymal Transition in Cancer: Insights Into Therapeutic Targets and Clinical Implications. MedComm. 2025; 6: e70333. https://doi.org/10.1002/mco2.70333

[18] Wan W, Ao X, Chen Q, Yu Y, Ao L, Xing W, et al. METTL3/IGF2BP3 axis inhibits tumor immune surveillance by upregulating N^6-methyladenosine modification of PD-L1 mRNA in breast cancer. Molecular Cancer. 2022; 21: 60. https://doi.org/10.1186/s12943-021-01447-y

[19] Ouyang P, Li K, Xu W, Chen C, Shi Y, Tian Y, et al. METTL3 recruiting M2-type immunosuppressed macrophages by targeting m6A-SNAIL-CXCL2 axis to promote colorectal cancer pulmonary metastasis. Journal of Experimental & Clinical Cancer Research : CR. 2024; 43: 111. https://doi.org/10.1186/s13046-024-03035-6

[20] Miyake K, Costa Cruz PH, Nagatomo I, Kato Y, Motooka D, Satoh S, et al. A cancer-associated METTL14 mutation induces aberrant m6A modification, affecting tumor growth. Cell Reports. 2023; 42: 112688. https://doi.org/10.1016/j.celrep.2023.112688

[21] Li L, Zeng J, He S, Yang Y, Wang C. METTL14 decreases FTH1 mRNA stability via m6A methylation to promote sorafenib-induced ferroptosis of cervical cancer. Cancer Biology & Therapy. 2024; 25: 2349429. https://doi.org/10.1080/15384047.2024.2349429

[22] Zehentner S, Reiner AT, Grimm C, Somoza V. The Role of Bitter Taste Receptors in Cancer: A Systematic Review. Cancers. 2021; 13: 5891. https://doi.org/10.3390/cancers13235891

[23] Zheng M, Zhou J, Wang Y. Primary cilia in cancer: structures, functions, mechanisms, and therapeutic implications. Cancer Biology & Medicine. 2025; 22: 1455–1472. https://doi.org/10.20892/j.issn.2095-3941.2025.0340

[24] Li W, Xie R, Chen H, Lin J, Zhong M, Zhang J, et al. METTL1-mediated m^7G tRNA modification drives papillary thyroid cancer progression and metastasis by regulating the codon-specific translation of TNF-α. Cell Death & Disease. 2025; 16: 378. https://doi.org/10.1038/s41419-025-07716-8

[25] Wei W, Zhang ZY, Shi B, Cai Y, Zhang HS, Sun CL, et al. METTL16 promotes glycolytic metabolism reprogramming and colorectal cancer progression. Journal of Experimental & Clinical Cancer Research : CR. 2023; 42: 151. https://doi.org/10.1186/s13046-023-02732-y

[26] Davydova E, Shimazu T, Schuhmacher MK, Jakobsson ME, Willemen HLDM, Liu T, et al. The methyltransferase METTL9

mediates pervasive 1-methylhistidine modification in mammalian proteomes. Nature Communications. 2021; 12: 891. https://doi.org/10.1038/s41467-020-20670-7

[27] Markowitz J, Carson WE, 3rd. Review of S100A9 biology and its role in cancer. Biochimica et Biophysica Acta. 2013; 1835: 100–109. https://doi.org/10.1016/j.bbcan.2012.10.003

[28] Rai NK, Venugopal H, Rajesh R, Ancha P, Venkatesh S. Mitochondrial complex-1 as a therapeutic target for cardiac diseases. Molecular and Cellular Biochemistry. 2025; 480: 869–890. https://doi.org/10.1007/s11010-024-05074-1

[29] Fan W, Xing Y, Yan S, Liu W, Ning J, Tian F, et al. DUSP5 regulated by YTHDF1-mediated m6A modification promotes epithelial-mesenchymal transition and EGFR-TKI resistance via the TGF-β/Smad signaling pathway in lung adenocarcinoma. Cancer Cell International. 2024; 24: 208. https://doi.org/10.1186/s12935-024-03382-6

[30] Wang S, Li Y, Jin K, Suda K, Li R, Zhang H, et al. PSME3 promotes lung adenocarcinoma development by regulating the TGF-β/SMAD signaling pathway. Translational Lung Cancer Research. 2024; 13: 1331–1345. https://doi.org/10.21037/tlcr-24-340

[31] Miao T, Zhang Y, Tian F, Xu X, Wei Q, Jiang X, et al. Down-regulation of MFNG promotes the metastatic potential of lung adenocarcinoma by regulating TGF-β/Smad signaling. iscience. 2025; 28: 113647. https://doi.org/10.1016/j.isci.2025.113647

[32] Topper MJ, Vaz M, Chiappinelli KB, DeStefano Shields CE, Niknafs N, Yen RWC, et al. Epigenetic Therapy Ties MYC Depletion to Reversing Immune Evasion and Treating Lung Cancer. Cell. 2017; 171: 1284–1300.e21. https://doi.org/10.1016/j.cell.2017.10.022

[33] Jones PA, Ohtani H, Chakravarthy A, De Carvalho DD. Epigenetic therapy in immune-oncology. Nature Reviews. Cancer. 2019; 19: 151–161. https://doi.org/10.1038/s41568-019-0109-9

[34] Wang Y, Zhang L, Zhou F. Cuproptosis: a new form of programmed cell death. Cellular & Molecular Immunology. 2022; 19: 867–868. https://doi.org/10.1038/s41423-022-00866-1

[35] Li Y, Du Y, Zhou Y, Chen Q, Luo Z, Ren Y, et al. Iron and copper: critical executioners of ferroptosis, cuproptosis and other forms of cell death. Cell Communication and Signaling : CCS. 2023; 21: 327. https://doi.org/10.1186/s12964-023-01267-1

[36] An J, Song W, Wang Q, Tan B, Fei X, Wang R, et al. Role of the SPI1/CDKN2A/p53 signaling pathway in cuproptosis of lung adenocarcinoma cells. Oncology Letters. 2025; 30: 353. https://doi.org/10.3892/ol.2025.15099

[37] Yang W, Wang Y, Huang Y, Yu J, Wang T, Li C, et al. 4-Octyl itaconate inhibits aerobic glycolysis by targeting GAPDH to promote cuproptosis in colorectal cancer. Biomedicine & Pharmacotherapy = Biomedecine & Pharmacotherapie. 2023; 159: 114301. https://doi.org/10.1016/j.biopha.2023.114301

[38] Hu Y, Liu H, Tan X, Wu X. Knocking Down Ferredoxin 1 Inhibits the Progression of Colorectal Cancer and Regulates Cuproptosis via Mediating the Hippo Signaling Pathway. Molecular Carcinogenesis. 2025; 64: 911–922. https://doi.org/10.1002/mc.23897

[39] Huang Y, Shan G, Yi Y, Liang J, Hu Z, Bi G, et al. FSCN1 induced PTPRF-dependent tumor microenvironment inflammatory reprogramming promotes lung adenocarcinoma progression via regulating macrophagic glycolysis. Cellular Oncology (Dordrecht, Netherlands). 2022; 45: 1383–1399. https://doi.org/10.1007/s13402-022-00726-0

[40] Wang L, Li Q, Sun Y, Wang S, Fu X, Wang X, et al. Tumor-derived immunoglobulin-like transcript 3 inhibition reshapes the immunosuppressive tumor microenvironment and potentiates programmed cell death ligand 1 blockade immunotherapy in lung adenocarcinoma. Translational Oncology. 2025; 56: 102381. https://doi.org/10.1016/j.tranon.2025.102381

[41] Li Y, Liu Y, Wang K, Xue D, Huang Y, Tan Z, et al. STK24 Promotes Progression of LUAD and Modulates the Immune Microenvironment. Mediators of Inflammation. 2023; 2023: 8646088. https://doi.org/10.1155/2023/8646088

[42] Sun C, Wang J, Li H, Liu L, Lin Y, Zhang L, et al. METTL14 regulates $CD8^{+}$T-cell activation and immune responses to anti-PD-1 therapy in lung cancer. World Journal of Surgical Oncology. 2024; 22: 128. https://doi.org/10.1186/s12957-024-03402-9

[43] Wu X, Zhu Z, Zhang J, Tian M, Zhao P. Progress in understanding the regulatory mechanisms of immune checkpoint proteins PD-1 and PD-L1 expression. Clinical & Translational Oncology : Official Publication of the Federation of Spanish Oncology Societies and of the National Cancer Institute of Mexico. 2025; 27: 3261–3271. https://doi.org/10.1007/s12094-024-03835-4

[44] Mondal K, Posa MK, Shenoy RP, Roychoudhury S. KRAS Mutation Subtypes and Their Association with Other Driver Mutations in Oncogenic Pathways. Cells. 2024; 13: 1221. https://doi.org/10.3390/cells13141221

[45] Ghosh S, Bhuniya T, Dey A, Koley M, Roy P, Bera A, et al. An Updated Review on KRAS Mutation in Lung Cancer (NSCLC) and Its Effects on Human Health. Applied Biochemistry and Biotechnology. 2024; 196: 4661–4678. https://doi.org/10.1007/s12010-023-04748-8